arXiv:1606.00412v1 [physics.optics] 30 May 2016

Spectral Singularities in the TE and TM modes of a $\mathcal{PT}$-Symmetric Slab System: Optimal conditions for realizing a CPA-Laser

Ali Mostafazadeh* and Mustafa Sarısaman†

Departments of Mathematics and Physics, Koç University,
34450 Sarıyer, Istanbul, Turkey

Abstract

Among the interesting outcomes of the study of the physical applications of spectral singularities in $\mathcal{PT}$-symmetric optical systems is the discovery of CPA-lasers. These are devices that act both as a threshold laser and a coherent perfect absorber (CPA) for the same values of their physical parameters. Unlike a homogeneous slab that is made to act as a CPA, a slab CPA-laser would absorb the incident waves coming from the left and right of the device provided that they have appropriate intensity and phase contrasts. We provide a comprehensive study of one of the simplest experimentally accessible examples of a CPA-laser, namely a $\mathcal{PT}$-symmetric optical slab system consisting of a balanced pair of adjacent or separated gain and loss components. In particular, we give a closed form expression describing the spectral singularities of the system which correspond to its CPA-laser configurations. We determine the intensity and phase contrasts for the TE and TM waves that are emitted (absorbed) whenever the slab acts as a laser (CPA). We also investigate the behavior of the time-averaged energy density $\langle u\rangle$ and Poynting vector $\langle\vec{S}\rangle$ for these waves. This is necessary for determining the optimal values of the physical parameters of the system that make it act as a CPA-laser. These turn out to correspond to situations where the separation distance s between the gain and loss layers is an odd multiple of a characteristic length scale s_0. A curious by-product of our study is that, except for the cases where s is an even integer multiple of s_0, there is a critical angle of polarization beyond which the energy of the waves emitted from the lossy layer can be larger than the energy of those emitted from the gain layer.

PACS numbers: 03.65.Nk, 42.25.Bs, 42.60.Da, 24.30.Gd

Keywords: Spectral singularity, $\mathcal{PT}$-symmetry, laser threshold condition, coherent perfect absorption, CPA-laser

*E-mail address: amostafazadeh@ku.edu.tr
†E-mail address: msarisaman@ku.edu.tr

1 Introduction

A basic fact about lasers is that they begin functioning once the gain coefficient g of the laser material exceeds a critical value known as the threshold gain $g_\star$. The relation $g = g_\star$ is therefore called the 'laser threshold condition' [1]. A few years ago [2] it was noticed that this condition coincided with the requirement that the continuous spectrum of the corresponding optical potential includes certain points known to mathematicians as spectral singularities [3, 4]. Spectral singularities entered into physics literature as mathematical obstructions [5, 6, 7] to a Hermitization procedure developed to construct unitary quantum systems using certain non-Hermitian Hamiltonian operators [8, 9]. Spectral singularities turn out to have an interesting physical meaning [10]; they correspond to a special class of scattering states with a real and positive energy that behave exactly like resonances. This observation has led to a detailed study of the physical aspects of spectral singularities [11, 12, 13, 14, 15, 16, 17, 18, 19, 20, 21, 22] and their nonlinear generalizations [23, 24, 25, 26]. Ref. [27] gives a brief survey of developments in the subject.

An interesting application of spectral singularities is in the description of the phenomenon of coherent perfect absorption (CPA) which is also called antilasing [28, 29, 30, 31, 32]. It turns out that there are special circumstances where an optical potential absorbs certain incident coherent waves. Given an optical potential v supporting a spectral singularity, the time-reversed optical system determined by the complex-conjugate of v displays CPA. An interesting situation is when a spectral singularity accompanies its time-reversal [17]. This happens for $\mathcal{PT}$-symmetric scattering potentials [29] and corresponds to a peculiar optical device that functions as a laser emitting coherent waves except when it is subject to certain incident coherent waves in which case it acts as an absorber. It is, therefore, called a CPA-laser. Today, CPA-lasers are theoretical constructs awaiting experimental realization.

The discovery of CPA-lasers is one of the most notable by-products of the recent interest in the manifestations and applications of $\mathcal{PT}$-symmetric potentials in optics [33, 34, 35, 36]. The role of $\mathcal{PT}$-symmetry in the context of CPA-lasers is similar to its role in the study of unidirectional indivisibility [37]. $\mathcal{PT}$-symmetry implies that the condition for the emergence of a spectral singularity coincides with that of its time-reversal [29]. This makes $\mathcal{PT}$-symmetric CPA-lasers the primary examples of CPA-lasers [17]. The same holds in the study of unidirectional invisibility. Because under $\mathcal{PT}$ the equations governing this effect are mapped to an equivalent set of equations, $\mathcal{PT}$-symmetric unidirectionally invisible potentials have a much simpler structure [38].

A basic problem in making a CPA-laser to act as a CPA is that the waves incident onto the device will not be absorbed unless they have correct amplitude and phase properties. This does not cause a major difficulty for a (non-lasing) CPA made out of a homogeneous slab of lossy material such as those considered in Refs. [31, 39], for the following reasons.

1. The optical potential for a homogeneous slab is $\mathcal{P}$-invariant, where $\mathcal{P}$ is the reflection about the plane parallel to the slab that passes through its center.

2. The equations governing the spectral singularities are $\mathcal{P}$-invariant [10, 2, 23].

These imply that the incoming waves from the left and right of the slab are absorbed provided that they have identical amplitude and phase. In contrast, the optical potential associated with a

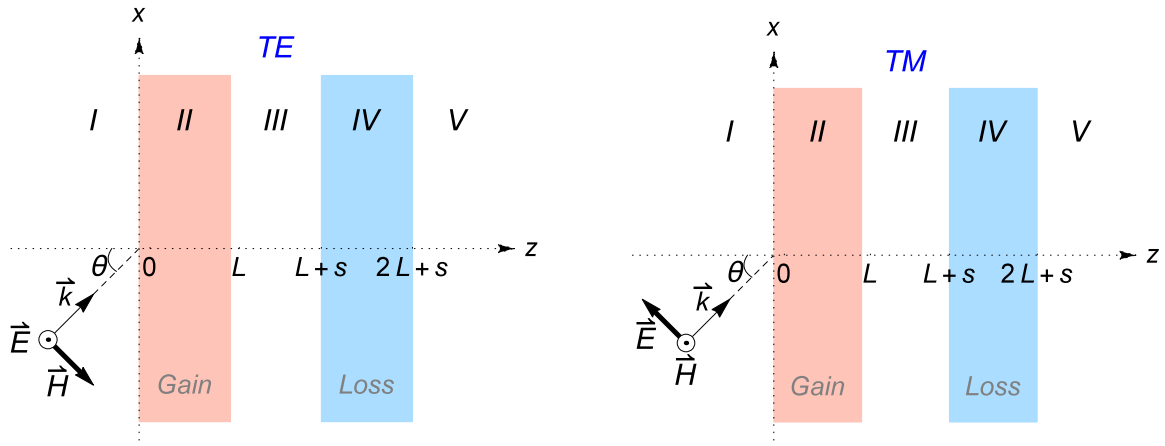

Figure 1: (Color online) TE (on the left) and TM (on the right) modes of a slab system consisting of a pair of gain and loss layers of thickness L placed a distance s apart in vacuum. The symbols I, II, III, IV, and V respectively label the regions of the space corresponding to $z<0$, $0<z<L$, $L<z<L+s$, $L+s<z<2L+s$, and $z>2L+s$.

CPA-laser (with planar symmetry) is never $\mathcal{P}$-invariant and the amplitude and phase properties of the absorbed waves depend on the details of the corresponding optical potential.

Recently, we have investigated the behavior of spectral singularities in the oblique TE (transverse electric) and TM (transverse magnetic) modes of an infinite planar slab of homogeneous gain (or lossy) medium and determined the laser threshold and CPA conditions for these modes [39]. This revealed a number of unusual phenomena related to the behavior of the energy density and Poynting vector for the TM modes with an incidence angle larger than the Brewster's angle. In the present article we use a similar approach to study a $\mathcal{PT}$-symmetric planar slab system that consists of a pair of balanced gain and loss layers of thickness L separated by a distance $s\geq 0$, as depicted in Fig. 1. Unlike the homogeneous slab of Ref. [39], this system is capable of serving as a CPA-laser. By studying the spectral singularities in its TE and TM modes, we obtain all possible configurations of this system that support CPA-laser action. In order to determine the practically most desirable choices among these, we examine the behavior of the energy density and Poynting vector for the spectrally singular TE and TM waves. We also give a complete solution for the problem of finding the intensity and phase contrasts that make the system absorb the incident waves. This provides valuable information for a possible experimental realization of a slab CPA-laser.

The organization of the article is as follows. In Sec. 2, we determine the explicit form of the TE and TM waves for the general case where the layers consist of arbitrary homogeneous optical material. In Sec. 3 we compute the transfer matrix for the system and derive an analytic expression for the condition of the presence of spectral singularities. In Sec. 4 we confine our attention to the $\mathcal{PT}$-symmetric case where the system consists of layers with balanced gain and loss. In Sec. 5 we investigate the effects of dispersion. In Sec. 6 we obtain explicit expressions for the spectrally singular TE and TM waves and examine the behavior of their energy density and the Poynting vector. In Sec. 7 we give the amplitude and phase conditions necessary for our $\mathcal{PT}$-symmetric CPA-laser to act as a perfect absorber, and in Sec. 8 we present our concluding

remarks.

2 TE and TM Modes of a Parallel Pair of Slabs

Consider the system depicted in Fig. 1. Suppose that the regions *II* and *IV* are respectively filled with gain and loss material having constant complex refractive indices $\mathfrak{n}_1$ and $\mathfrak{n}_2$. Let $\vec{\mathcal{E}}$ and $\vec{\mathcal{H}}$ denote the electric and magnetic fields interacting with this system, and

$$\mathfrak{z}(z) := \begin{cases} \mathfrak{n}_1^2 & \text{for} \quad z \in II, \\ \mathfrak{n}_2^2 & \text{for} \quad z \in IV, \\ 1 & \text{otherwise.} \end{cases} \tag{1}$$

Then Maxwell's equations for the time-harmonic electromagnetic fields, $\vec{\mathcal{E}}(\vec{r},t) = e^{-i\omega t}\vec{E}(\vec{r})$ and $\vec{\mathcal{H}}(\vec{r},t) = e^{-i\omega t}\vec{H}(\vec{r})$, take the form

$$\left[\nabla^2 + k^2\mathfrak{z}(z)\right]\vec{E}(\vec{r}) = 0, \qquad \vec{H}(\vec{r}) = -\frac{i}{kZ_0}\vec{\nabla}\times\vec{E}(\vec{r}), \tag{2}$$

$$\left[\nabla^2 + k^2\mathfrak{z}(z)\right]\vec{H}(\vec{r}) = 0, \qquad \vec{E}(\vec{r}) = \frac{iZ_0}{k\mathfrak{z}(z)}\vec{\nabla}\times\vec{H}(\vec{r}), \tag{3}$$

where $\vec{r} := (x,y,z)$, $k := \omega/c$ is the wavenumber, $c := 1/\sqrt{\mu_0\varepsilon_0}$ is the the speed of light in vacuum, and $Z_0 := \sqrt{\mu_0/\varepsilon_0}$, ε_0, and μ_0 are respectively the impedance, permittivity, and permeability of the vacuum.

The TE and TM waves correspond to the solutions of (2) and (3) for which $\vec{E}(\vec{r})$ and $\vec{H}(\vec{r})$ are respectively parallel to the surface of the slabs. We use a coordinate system in which they are aligned along the y-axis. Suppose that for $z<0$, $\vec{E}(\vec{r})$ (respectively $\vec{H}(\vec{r})$) coincides with a plane wave with wavevector $\vec{k}$ in the x-z plane, i.e.,

$$\vec{k} = k_x\hat{e}_x + k_z\hat{e}_z, \qquad k_x := k\sin\theta, \qquad k_z := k\cos\theta, \tag{4}$$

where $\hat{e}_x, \hat{e}_y$, and $\hat{e}_z$, are respectively the unit vectors along the x-, y- and z-axes, and θ is the incidence angle (See Fig. 1.) Then the electric field for the TE waves and the magnetic field for the TM waves are respectively given by

$$\vec{E}(\vec{r}) = \mathscr{E}(z)e^{ik_x x}\hat{e}_y, \qquad \vec{H}(\vec{r}) = \mathscr{H}(z)e^{ik_x x}\hat{e}_y, \tag{5}$$

where $\mathscr{E}$ and $\mathscr{H}$ are solutions of the Schrödinger equation

$$-\psi''(z) + v(z)\psi(z) = k^2\psi(z), \qquad z \notin \{0, L, L+s, 2L+s\}, \tag{6}$$

for the potential

$$v(z) := k^2[1 + \sin^2\theta - \mathfrak{z}(z)].$$

Because $v(z)$ is a piecewise constant potential, we can easily solve (6) to obtain

$$\psi(z) := \begin{cases} a_1\, e^{ik_z z} + b_1\, e^{-ik_z z} & \text{for} \quad z \in I, \\ a_2\, e^{i\tilde{k}_1 z} + b_2\, e^{-i\tilde{k}_1 z} & \text{for} \quad z \in II, \\ a_3\, e^{ik_z z} + b_3\, e^{-ik_z z} & \text{for} \quad z \in III, \\ a_4\, e^{i\tilde{k}_2 z} + b_4\, e^{-i\tilde{k}_2 z} & \text{for} \quad z \in IV, \\ a_5\, e^{ik_z z} + b_5\, e^{-ik_z z} & \text{for} \quad z \in V, \end{cases} \tag{7}$$

where a_i and b_i, with $i = 1, 2, 3, 4, 5$, are complex coefficients, and

$$\tilde{k}_j := k\sqrt{\mathfrak{n}_j^2 - \sin^2\theta} = k_z\tilde{\mathfrak{n}}_j, \qquad\qquad \tilde{\mathfrak{n}}_j := \sec\theta\,\sqrt{\mathfrak{n}_j^2 - \sin^2\theta}. \tag{8}$$

Substituting (5) in the second equation in (2) and (3), we can find the magnetic field for the TE waves and the electric field for the TM waves inside and outside the slabs. We then impose the appropriate boundary conditions for the problem to relate the coefficients a_i and b_i. These amount to the requirement that the tangential components of $\vec{E}$ and $\vec{H}$ must be continuous functions of z at $z = 0$, $z = L$, $z = L + s$ and $z = 2L + s$. Table 1 gives explicit expressions for the components of the electric and magnetic fields, and Table 2 lists the corresponding boundary conditions. They involve the following quantities.

TE-Fields	TM-Fields
$E_x = E_z = H_y = 0$	$E_y = H_x = H_z = 0$
$E_y = \mathscr{E}(z)\, e^{ik_x x}$	$E_x = \dfrac{Z_0\,\mathscr{F}(z)}{\mathfrak{z}(z)}\,\mathscr{T}(x,z)$
$H_x = -\dfrac{\mathscr{F}(z)}{Z_0}\,\mathscr{T}(x,z)$	$E_z = -\dfrac{Z_0\sin\theta\, e^{ik_x x}\mathscr{H}(z)}{\mathfrak{z}(z)}$
$H_z = \dfrac{\sin\theta\, e^{ik_x x}\mathscr{E}(z)}{Z_0}$	$H_y = \mathscr{H}(z)\, e^{ik_x x}$

Table 1: Components of the TE and TM fields in cartesian coordinates. Here $\mathscr{E}(z)$ is given by the right-hand side of (7), and $\mathscr{F}(z)$ and $\mathscr{T}(x,z)$ are respectively defined by (9) and (10).

$z = 0$	$a_1 + b_1 = a_2 + b_2, \quad b_1 - a_1 = \mathfrak{u}_1(b_2 - a_2)$
$z = L$	$a_2 e^{i\tilde{k}_1 L} + b_2 e^{-i\tilde{k}_1 L} = a_3 e^{ik_z L} + b_3 e^{-ik_z L}$ $\mathfrak{u}_1(a_2 e^{i\tilde{k}_1 L} - b_2 e^{-i\tilde{k}_1 L}) = a_3 e^{ik_z L} - b_3 e^{-ik_z L}$
$z = L + s$	$a_3 e^{ik_z(L+s)} + b_3 e^{-ik_z(L+s)} = a_4 e^{i\tilde{k}_2(L+s)} + b_4 e^{-i\tilde{k}_2(L+s)}$ $a_3 e^{ik_z(L+s)} - b_3 e^{-ik_z(L+s)} = \mathfrak{u}_2(a_4 e^{i\tilde{k}_2(L+s)} - b_4 e^{-i\tilde{k}_2(L+s)})$
$z = 2L + s$	$a_4 e^{i\tilde{k}_2(2L+s)} + b_4 e^{-i\tilde{k}_2(2L+s)} = a_5 e^{ik_z(2L+s)} + b_5 e^{-ik_z(2L+s)}$ $\mathfrak{u}_2(a_4 e^{i\tilde{k}_2(2L+s)} - b_4 e^{-i\tilde{k}_2(2L+s)}) = a_5 e^{ik_z(2L+s)} - b_5 e^{-ik_z(2L+s)}$

Table 2: Boundary conditions for the TE and TM waves.

$$\mathscr{F}(z) := \begin{cases} a_1\, e^{ik_z z} - b_1\, e^{-ik_z z} & \text{for} \quad z \in I, \\ a_2\, e^{i\tilde{k}_1 z} - b_2\, e^{-i\tilde{k}_1 z} & \text{for} \quad z \in II, \\ a_3\, e^{ik_z z} - b_3\, e^{-ik_z z} & \text{for} \quad z \in III, \\ a_4\, e^{i\tilde{k}_2 z} - b_4\, e^{-i\tilde{k}_2 z} & \text{for} \quad z \in IV, \\ a_5\, e^{ik_z z} - b_5\, e^{-ik_z z} & \text{for} \quad z \in V, \end{cases} \tag{9}$$

$$\mathscr{T}(x,z) := \begin{cases} \sqrt{\mathfrak{n}_1^2 - \sin^2\theta}\, e^{ik_x x} & \text{for } z \in II, \\ \sqrt{\mathfrak{n}_2^2 - \sin^2\theta}\, e^{ik_x x} & \text{for } z \in IV, \\ \cos\theta\, e^{ik_x x} & \text{otherwise}, \end{cases} \tag{10}$$

$$\mathfrak{u}_j := \begin{cases} \tilde{\mathfrak{n}}_j = \sec\theta\, \sqrt{\mathfrak{n}_j^2 - \sin^2\theta} & \text{for TE waves}, \\ \dfrac{\tilde{\mathfrak{n}}_j}{\mathfrak{n}_j^2} = \mathfrak{n}_j^{-2} \sec\theta\, \sqrt{\mathfrak{n}_j^2 - \sin^2\theta} & \text{for TM waves}. \end{cases} \tag{11}$$

3 Transfer Matrix and Spectral Singularities

Transfer matrix formalism provides an effective method of computing the scattering properties of multilayer systems. For the system we consider, the transfer matrix of the slabs placed in regions *II* and *IV* and the transfer matrix of the whole system are respectively the 2×2 matrices $\mathbf{M}_1$, $\mathbf{M}_2$, and $\mathbf{M} = [M_{ij}]$ satisfying

$$\begin{bmatrix} a_3 \\ b_3 \end{bmatrix} = \mathbf{M}_1 \begin{bmatrix} a_1 \\ b_1 \end{bmatrix}, \qquad \begin{bmatrix} a_5 \\ b_5 \end{bmatrix} = \mathbf{M}_2 \begin{bmatrix} a_3 \\ b_3 \end{bmatrix}, \qquad \begin{bmatrix} a_5 \\ b_5 \end{bmatrix} = \mathbf{M} \begin{bmatrix} a_1 \\ b_1 \end{bmatrix}.$$

These in particular imply the well-known composition relation,

$$\mathbf{M} = \mathbf{M}_2 \mathbf{M}_1. \tag{12}$$

Ref. [39] gives an explicit expression for $\mathbf{M}_1$. We can easily compute $\mathbf{M}_2$ using this expression and the transformation property of the transfer matrices under translations, $z \xrightarrow{T_a} z - a$. In terms of the entries M_{ij} of a generic transfer matrix, this takes the form [40]:

$$M_{11} \xrightarrow{T_a} M_{11}, \qquad M_{12} \xrightarrow{T_a} e^{-2iak_z} M_{12}, \qquad M_{21} \xrightarrow{T_a} e^{2iak_z} M_{21}, \qquad M_{22} \xrightarrow{T_a} M_{22}.$$

Having $\mathbf{M}_1$ and $\mathbf{M}_2$ computed, we can determine $\mathbf{M}$ using (12). Here we only give the expression for M_{22}.

$$\begin{aligned} M_{22} &= \cos\mathfrak{a}_1 \cos\mathfrak{a}_2 \Big[1 - i\,\mathfrak{u}_1^+ \tan\mathfrak{a}_1 - i\,\mathfrak{u}_2^+ \tan\mathfrak{a}_2 + \\ &\qquad (\mathfrak{u}_1^- \mathfrak{u}_2^- e^{2ik_z s} - \mathfrak{u}_1^+ \mathfrak{u}_2^+) \tan\mathfrak{a}_1 \tan\mathfrak{a}_2 \Big] e^{2ik_z L}, \end{aligned} \tag{13}$$

where we have introduced

$$\mathfrak{a}_j := k_z L \tilde{\mathfrak{n}}_j, \qquad\qquad \mathfrak{u}_j^{\pm} := \frac{1}{2}\left(\mathfrak{u}_j \pm \mathfrak{u}_j^{-1}\right).$$

As noted in Refs. [7, 10], spectral singularities correspond to the real values of the wavenumber k for which $M_{22} = 0$. In light of (13), we can express this equation in the form

$$e^{2i\mathfrak{a}_2} = \frac{(\mathfrak{u}_1^2-1)(\mathfrak{u}_2^2-1)e^{2ik_z s}(e^{2i\mathfrak{a}_1}-1) + (\mathfrak{u}_2+1)^2[(\mathfrak{u}_1+1)^2 - (\mathfrak{u}_1-1)^2 e^{2i\mathfrak{a}_1}]}{(\mathfrak{u}_1^2-1)(\mathfrak{u}_2^2-1)e^{2ik_z s}(e^{2i\mathfrak{a}_1}-1) + (\mathfrak{u}_2-1)^2[(\mathfrak{u}_1+1)^2 - (\mathfrak{u}_1-1)^2 e^{2i\mathfrak{a}_1}]}. \tag{14}$$

For a bilayer slab, $s=0$, and this relation takes the following simpler form

$$e^{2i\mathfrak{a}_2}=\left(\frac{\mathfrak{u}_2+1}{\mathfrak{u}_2-1}\right)\left[\frac{e^{2i\mathfrak{a}_1}(\mathfrak{u}_1-1)(\mathfrak{u}_2-\mathfrak{u}_1)+(\mathfrak{u}_1+1)(\mathfrak{u}_1+\mathfrak{u}_2)}{e^{2i\mathfrak{a}_1}(\mathfrak{u}_1-1)(\mathfrak{u}_1+\mathfrak{u}_2)+(\mathfrak{u}_1+1)(\mathfrak{u}_2-\mathfrak{u}_1)}\right]. \tag{15}$$

For $\mathfrak{n}_1=1$ (similarly $\mathfrak{n}_2=1$), this relation reduces to the condition for the presence of a spectral singularity in the TE and TM modes of a homogeneous slab [39]. For normally incident waves, where $\theta=0$, it reproduces the results of Ref. [17].

4 $\mathcal{PT}$-Symmetric Configurations

Consider the situation that the gain and loss components of our system balance one another, i.e., $\mathfrak{n}_2^*=\mathfrak{n}_1=:\mathfrak{n}$. Then it is $\mathcal{PT}$-symmetric, and we have

$$\tilde{\mathfrak{n}}_2^*=\tilde{\mathfrak{n}}_1=:\tilde{\mathfrak{n}},\qquad\qquad \mathfrak{u}_2^*=\mathfrak{u}_1=:\mathfrak{u},\qquad\qquad \mathfrak{a}_2^*=\mathfrak{a}_1=:\mathfrak{a}. \tag{16}$$

First we examine the case of a $\mathcal{PT}$-symmetric bilayer slab with adjacent gain and loss layers, i.e., set $s=0$. Then in view of (11) and (16), Eq. (15) takes the form

$$e^{2i\mathfrak{a}^*}=\left(\frac{\tilde{\mathfrak{n}}^*+\mathfrak{n}^{*\ell}}{\tilde{\mathfrak{n}}^*-\mathfrak{n}^{*\ell}}\right)\left[\frac{e^{2i\mathfrak{a}}(\tilde{\mathfrak{n}}^*\mathfrak{n}^\ell-\tilde{\mathfrak{n}}\,\mathfrak{n}^{*\ell})(\tilde{\mathfrak{n}}-\mathfrak{n}^\ell)+(\tilde{\mathfrak{n}}\,\mathfrak{n}^{*\ell}+\tilde{\mathfrak{n}}^*\mathfrak{n}^\ell)(\mathfrak{n}^\ell+\tilde{\mathfrak{n}})}{e^{2i\mathfrak{a}}(\tilde{\mathfrak{n}}^*\mathfrak{n}^\ell+\tilde{\mathfrak{n}}\,\mathfrak{n}^{*\ell})(\tilde{\mathfrak{n}}-\mathfrak{n}^\ell)+(\tilde{\mathfrak{n}}^*\mathfrak{n}^\ell-\tilde{\mathfrak{n}}\,\mathfrak{n}^{*\ell})(\mathfrak{n}^\ell+\tilde{\mathfrak{n}})}\right], \tag{17}$$

where

$$\ell:=\begin{cases}0 & \text{for TE waves,}\\ 2 & \text{for TM waves.}\end{cases}$$

In order to clarify the physical meaning of (17), we expand both sides of this relation in powers of the imaginary part κ of $\mathfrak{n}$ and ignore quadratic and higher order terms. This yields a reliable approximation provided that

$$|\kappa|\ll\eta-1<\eta, \tag{18}$$

where η stands for the real part of $\mathfrak{n}$, so that

$$\mathfrak{n}=\eta+i\kappa. \tag{19}$$

Similarly, we use $\tilde\eta$ and $\tilde\kappa$ to denote the real and imaginary parts of $\tilde{\mathfrak{n}}$, respectively. To leading order in κ, we have

$$\tilde\eta\approx\sec\theta\sqrt{\eta^2-\sin^2\theta},\qquad\qquad \tilde\kappa\approx\frac{\sec\theta\,\eta\,\kappa}{\sqrt{\eta^2-\sin^2\theta}}. \tag{20}$$

Substituting $\tilde{\mathfrak{n}}=\tilde\eta+i\tilde\kappa$ in (17), making use of (20), and keeping the leading order terms in κ we can reduce (17) to the following pair of real equations.

$$g\approx\frac{\sqrt{\eta^2-\sin^2\theta}}{\eta L}\ln\left|\frac{2\eta^\ell\tilde\eta(\eta^{2\ell}+\tilde\eta^2)}{\sigma_\ell\,\tilde\kappa(\eta^{2\ell}-\tilde\eta^2)}\right|, \tag{21}$$

$$\lambda\approx\frac{8L\sqrt{\eta^2-\sin^2\theta}}{2m+1}. \tag{22}$$

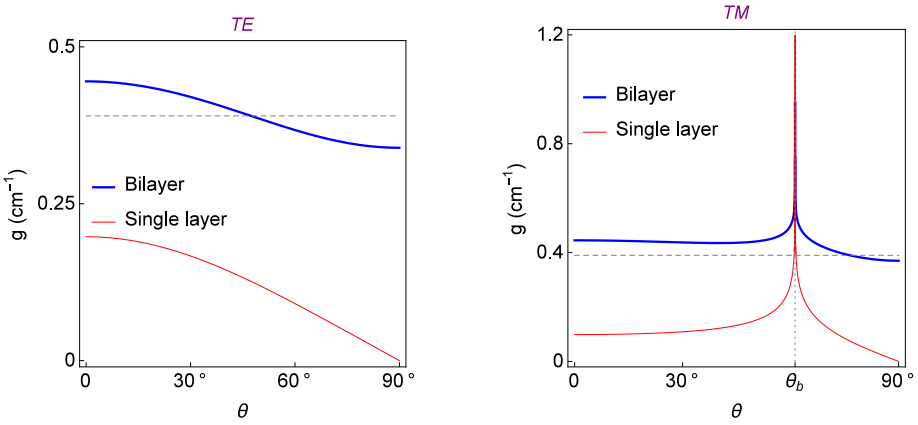

Figure 2: (Color online) Plots of the threshold gain coefficient g as a function of the incidence angle θ for the TE and TM modes of a homogenous active slab of thickness 25 cm (thin red curves) and a $\mathcal{PT}$-symmetric bilayer slab of layer thickness 25 cm (thick blue curves) made out of Nd:YAG crystals with $\eta = 1.8217$. θ_b labels the Brewster's angle and has the value 61.24°. The dotted horizontal line marks the experimental upper bound on the gain coefficient.

Here g is the gain coefficient given by

$$g := -2k\kappa = -\frac{4\pi\kappa}{\lambda}, \tag{23}$$

$\lambda := 2\pi/k$ is the wavelength, $m = 1, 2, 3, \cdots$ is a mode number, and

$$\sigma_\ell := \begin{cases} 1 & \text{for} \quad \ell = 0, \\ 2\sin^2\theta - \eta^2 & \text{for} \quad \ell = 2. \end{cases}$$

Equations (21) and (22) provide the laser threshold and phase conditions in the TE and TM modes of our $\mathcal{PT}$-symmetric bilayer slab provided that it is made out of typical optical material satisfying (18).

Figure 2 shows the graphs of the threshold gain coefficient g as a function of θ for a homogeneous slab of gain material and a $\mathcal{PT}$-symmetric bilayer slab made out of Nd:YAG crystals. The main difference is that the threshold gain coefficient for the latter does not tend to zero at the grazing angle ($\theta = 90°$).

Comparing the phase condition (22) for the $\mathcal{PT}$-symmetric bilayer with that of a homogeneous slab of thickness $2L$, we find that the value of λ for the latter is given by (22) if we change m to $m - 1/2$ (see [39]). Given that typically m takes very large values, the wavelength λ is essentially the same for the two slabs.

Next, we consider the general case, where the gain and loss components of our system are placed at a distance s apart. A similar analysis of (14) leads to the following expressions for the threshold gain coefficient and wavelength.

$$g \approx \frac{\sqrt{\eta^2 - \sin^2\theta}}{2\eta L} \ln\left[\frac{1 - \mathcal{A}_\ell - \sqrt{1 - 2\mathcal{A}_\ell}}{\mathcal{A}_\ell - \mathcal{B}_\ell}\right], \tag{24}$$

$$\lambda \approx \frac{4L\sqrt{\eta^2 - \sin^2\theta}}{m + \mathcal{C}_\ell}, \tag{25}$$

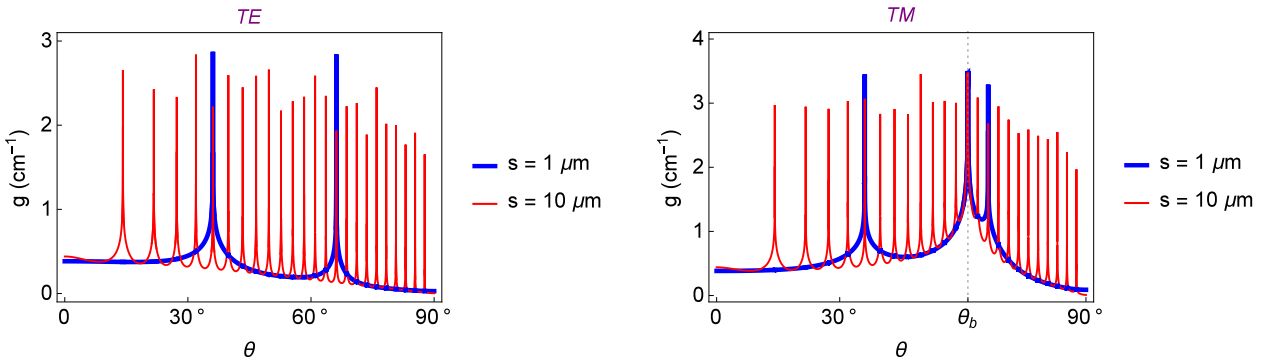

Figure 3: (Color online) Plots of gain coefficient g as a function of the incidence angle θ for the TE and TM modes of a $\mathcal{PT}$-symmetric two-slab system made out of Nd:YAG crystals with $\eta = 1.8217$, $L = 25$ mm, and separation distances $s = 1$ μm (thick blue curves) and $s = 10$ μm (thin red curves). For larger values of s there are more peaks, but the general behavior of g does not change.

where

$$\mathcal{A}_\ell := \frac{\sin^4(k_z s) + \tau_\ell^+ \sin^2(2k_z s)}{2[\sin^2(k_z s) + 4\tau_\ell^-]^2}, \qquad \mathcal{B}_\ell := \frac{(\tilde\eta^2 - \eta^{2\ell})\tilde\kappa\sigma_\ell \sin(2k_z s)}{(\tilde\eta^2 + \eta^{2\ell})^2[\sin^2(k_z s) + 4\tau_\ell^-]}, \qquad \tau_\ell^\pm := \frac{\tilde\eta^2\eta^{2\ell}}{(\tilde\eta^2 \pm \eta^{2\ell})^2},$$

$$\mathcal{C}_\ell := \frac{1}{\pi}\arccos\left\{\left[\frac{(1 - \mathcal{B}_\ell - \sqrt{1 - 2\mathcal{A}_\ell})\sin^2(k_z s)}{2\sqrt{(\mathcal{A}_\ell - \mathcal{B}_\ell)(1 - \mathcal{A}_\ell - \sqrt{1 - 2\mathcal{A}_\ell})}\,[\sin^2(k_z s) + 4\tau_\ell^-]}\right]\right\}.$$

We have checked that in the limit $s \to 0$, Eqs. (24) and (25) do actually tend to Eqs. (21) and (22).

Figs. 3 and 4 show the graphs of the threshold gain coefficient g as a function of θ for the TE and TM modes of a $\mathcal{PT}$-symmetric two-slab system for different separation distances s. The peaks are consequences of internal reflections in the gap between the two slabs. Their number is an increasing function of s. For $\theta \to 90°$, the presence of the gap changes the behavior of g drastically. Unlike for the case $s = 0$ and similarly to the single layer slab considered in Ref. [39], here g tends to zero as $\theta \to 90°$.

Fig. 5 shows the plots of the threshold gain coefficient g as a function of the separation distance s for different values of the incidence angle.

5 Inclusion of the Effects of Dispersion

In the preceding section we have ignored the fact that the index of refraction depends on the wavenumber k. In this section we consider the influence of the k-dependence of $\mathfrak{n}$ on the spectral singularities in the TE and TM modes of our $\mathcal{PT}$-symmetric two-slab system.

Suppose that the active material filling the left-hand (gain) layer is obtained by doping a host medium of refraction index n_0 and its refractive index satisfies the dispersion relation

$$\mathfrak{n}^2 = n_0^2 - \frac{\hat\omega_p^2}{\hat\omega^2 - 1 + i\hat\gamma\,\hat\omega}, \tag{26}$$

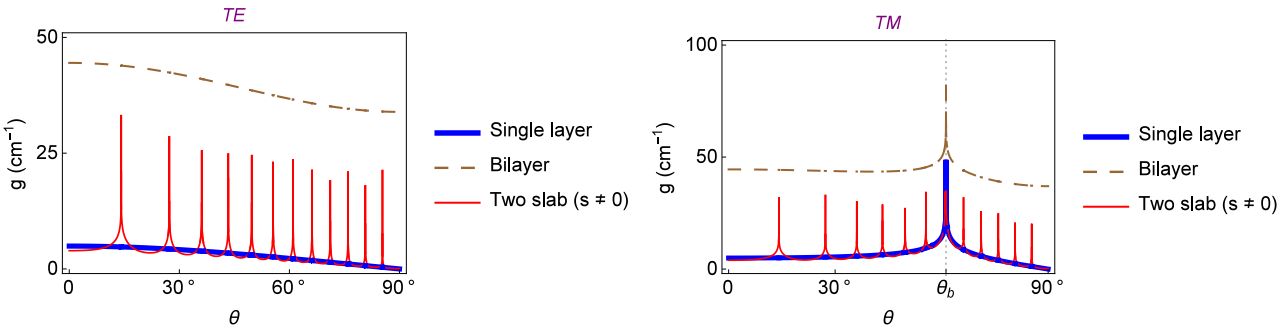

Figure 4: (Color online) Plots of the threshold gain coefficient g as a function of the incidence angle θ for single layer gain slab (thick blue curves), a $\mathcal{PT}$-symmetric bilayer slab (dashed curves), and a $\mathcal{PT}$-symmetric two-slab system (thin red curves) all made of Nd:YAG crystals. We have taken the thickness of the single layer slab to be 5 mm, while for the bilayer slab and the two-slab system we have set $L = 2.5$ mm. For the latter we have taken $s = 5$ μm.

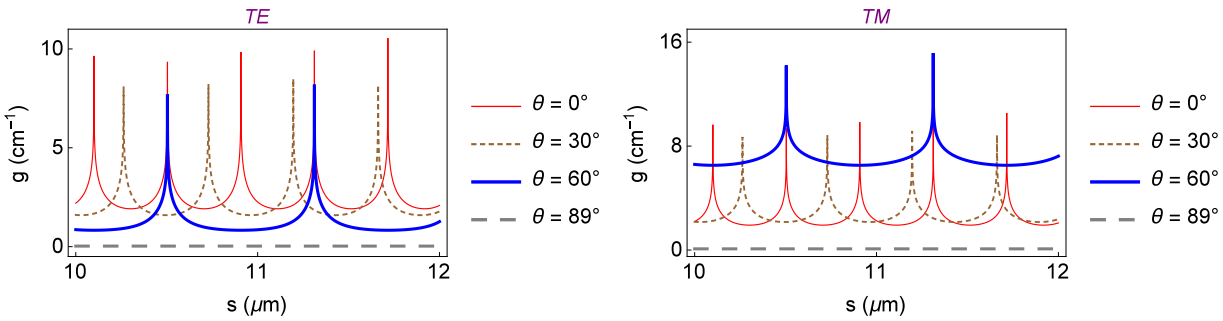

Figure 5: (Color online) Plots of the threshold gain coefficient g as a function of the separation distance s for the TE and TM modes of a $\mathcal{PT}$-symmetric two-slab system made out of Nd:YAG crystals with $\eta = 1.8217$ and $L = 5$ mm for various incidence angles θ. The number of peaks is a decreasing function of θ.

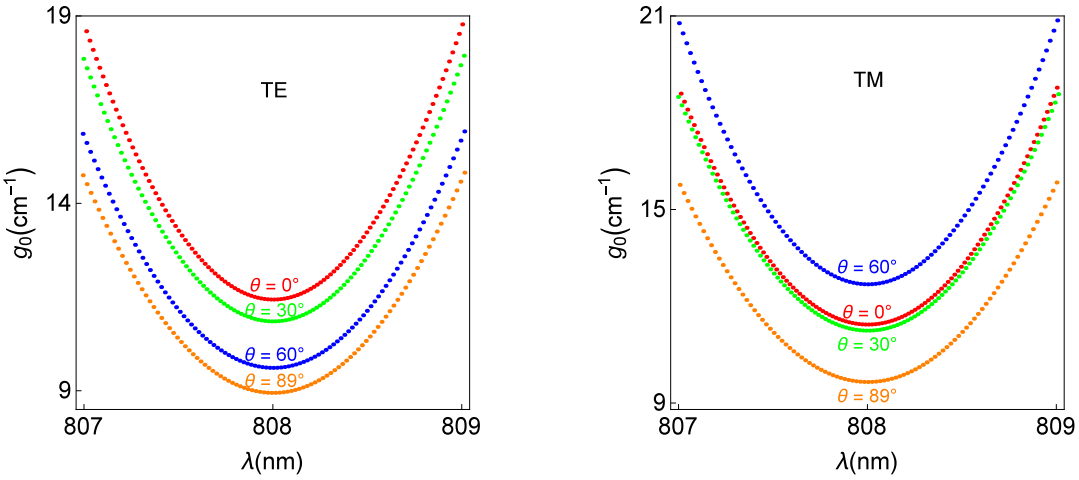

Figure 6: (Color online) The threshold gain g_0 and the wavelength λ for the spectral singularities in the TE and TM modes of a $\mathcal{PT}$-symmetric bilayer slab of layer thickness $L = 1$ cm made out of the gain medium (28) for different incidence angles θ. The minimum value of g_0 is obtained for the spectral singularities at the resonance wavelength. The threshold gain coefficient takes smaller values for larger incidence angles.

where $\hat{\omega} := \omega/\omega_0$, $\hat{\gamma} := \gamma/\omega_0$, $\hat{\omega}_p := \omega_p/\omega_0$, ω_0 is the resonance frequency, γ is the damping coefficient, and ω_p is the plasma frequency. We can express $\hat{\omega}_p^2$ in terms of the imaginary part κ_0 of $\mathfrak{n}$ at the resonance wavelength $\lambda_0 := 2\pi c/\omega_0$ according to $\hat{\omega}_p^2 = 2n_0\hat{\gamma}\kappa_0 + \mathcal{O}(\kappa_0^2)$, where $\mathcal{O}(\kappa_0^2)$ stands for the quadratic and higher order terms in κ_0, [2]. Substituting this equation in (26), using (19), and neglecting quadratic and higher order terms in κ_0, we obtain [15]

$$\eta \approx n_0 + \frac{\kappa_0\hat{\gamma}(1-\hat{\omega}^2)}{(1-\hat{\omega}^2)^2+\hat{\gamma}^2\hat{\omega}^2}, \qquad \kappa \approx \frac{\kappa_0\hat{\gamma}^2\hat{\omega}}{(1-\hat{\omega}^2)^2+\hat{\gamma}^2\hat{\omega}^2}. \tag{27}$$

At a resonance wavelength, (23) reads $\kappa_0 = -\lambda_0 g_0/4\pi$. Inserting this relation in (27) and making use of (19), (14) and (15), we can determine the λ and g_0 values for the spectral singularities. Figures 6 and 7 respectively show the location of the spectral singularities in the λ-g_0 plane for a $\mathcal{PT}$-symmetric bilayer with layer thickness $L = 1\,\text{cm}$ and a $\mathcal{PT}$-symmetric two-slab system with layer thickness $L = 2.5\,\text{cm}$ and the separation distance $s = 0.5\,\text{mm}$. Both of these are made of Nd:YAG crystals with the following specifications [1]:

$$n_0 = 1.8217, \qquad \lambda_1 = 808\,\text{nm}, \qquad \hat{\gamma} = 0.003094. \tag{28}$$

6 Spectrally Singular TE and TM Waves

Because spectral singularities are associated with the singularities of the reflection and transmission amplitudes [10], they correspond to solutions of the wave equation with purely outgoing boundary conditions. For the system we consider, these are characterized by

$$a_1 = b_5 = 0. \tag{29}$$

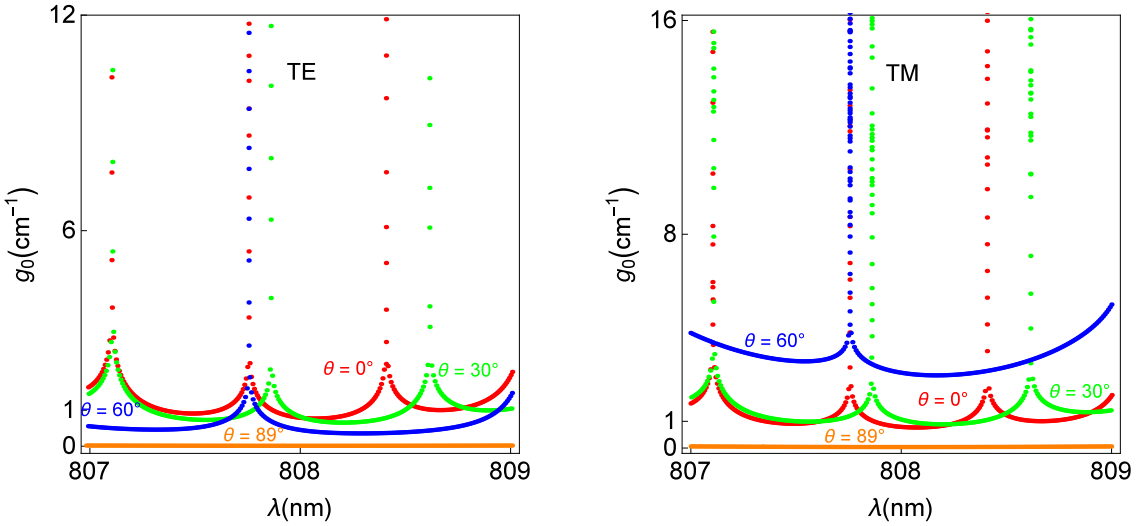

Figure 7: (Color online) The threshold gain g_0 and the wavelength λ for the spectral singularities in the TE and TM modes of a $\mathcal{PT}$-symmetric two-slab system with layer thickness $L = 2.5$ cm and separation distance $s = 0.5$ mm made out of the gain medium (28) for different incidence angles θ. There are certain wavelengths corresponding to extremely large values of g_0 where lasing is impossible. The number of these increases with the separation distance. As the incidence angle increases, g_0 decreases.

In this section we examine the TE and TM modes of our $\mathcal{PT}$-symmetric slab system that fulfill this condition. Following Ref. [39] we refer to them as 'singular waves' or 'singular modes'.

We begin our study of these modes by enforcing Eqs. (14) and (29), and the boundary conditions given in Table 2. This gives

$$a_5 = V_s(\tilde{\mathfrak{n}}_1, \tilde{\mathfrak{n}}_2, L)\, e^{-ik_z(2L+s)}\, b_1, \tag{30}$$

where for each $z \in \mathbb{R}$,

$$V_s(\tilde{\mathfrak{n}}_1, \tilde{\mathfrak{n}}_2, z) := U_1(\tilde{\mathfrak{n}}_1, z)e^{ik_z s} + \left(\frac{\mathfrak{u}_2 - 1}{\mathfrak{u}_2 + 1}\right) U_2(\tilde{\mathfrak{n}}_1, z)e^{-ik_z s}, \tag{31}$$

$$U_1(\tilde{\mathfrak{n}}, z) := \frac{1}{2}\left[U_+(\tilde{\mathfrak{n}}, z) + \mathfrak{u}\, U_-(\tilde{\mathfrak{n}}, z)\right], \tag{32}$$

$$U_2(\tilde{\mathfrak{n}}, z) := \frac{1}{2}(\mathfrak{u} + 1)\, U_+(\tilde{\mathfrak{n}}, z), \tag{33}$$

$$U_\pm(\tilde{\mathfrak{n}}, z) := \frac{1}{2\mathfrak{u}}\left[(\mathfrak{u} - 1)\, e^{ik_z z\tilde{\mathfrak{n}}} \pm (\mathfrak{u} + 1)\, e^{-ik_z z\tilde{\mathfrak{n}}}\right]. \tag{34}$$

Next we substitute (29) in the formulas given in Table 1 to obtain the explicit form of the

Spectrally Singular TE-Fields	Spectrally Singular TM-Fields
$E_x = E_z = H_y = 0$	$E_y = H_x = H_z = 0$
$E_y = b_1 e^{ik_x x} F^s_+(\tilde{\mathfrak{n}}_1, \tilde{\mathfrak{n}}_2, z)$	$E_x = b_1 Z_0 \cos\theta\, e^{ik_x x} F^s_-(\tilde{\mathfrak{n}}_1, \tilde{\mathfrak{n}}_2, z)$
$H_x = -\dfrac{b_1 \cos\theta}{Z_0}\, e^{ik_x x} F^s_-(\tilde{\mathfrak{n}}_1, \tilde{\mathfrak{n}}_2, z)$	$E_z = -b_1 Z_0 \sin\theta\, e^{ik_x x} \dfrac{F^s_+(\tilde{\mathfrak{n}}_1, \tilde{\mathfrak{n}}_2, z)}{\mathfrak{z}(z)}$
$H_z = \dfrac{b_1 \sin\theta}{Z_0}\, e^{ik_x x} F^s_+(\tilde{\mathfrak{n}}_1, \tilde{\mathfrak{n}}_2, z)$	$H_y = b_1 e^{ik_x x} F^s_+(\tilde{\mathfrak{n}}_1, \tilde{\mathfrak{n}}_2, z)$

Table 3: Components of the spectrally singular TE and TM fields in cartesian coordinates. Here $\tilde{\mathfrak{n}}_j$ and $F^s_\pm(\tilde{\mathfrak{n}}_1, \tilde{\mathfrak{n}}_2, z)$ are respectively defined by (8) and (35).

singular TE and TM waves. Table 3 gives the result of this calculation in terms of the functions:

$$F^s_\pm(\tilde{\mathfrak{n}}_1, \tilde{\mathfrak{n}}_2, z) := \begin{cases} \pm e^{-ik_z z} & \text{for} \quad z \in I, \\ \mathfrak{u}_1^{(1\mp 1)/2} U_\pm(\tilde{\mathfrak{n}}_1, z) & \text{for} \quad z \in II, \\ V_\pm(\tilde{\mathfrak{n}}_1, z - L) & \text{for} \quad z \in III, \\ \mathfrak{u}_2^{(1\mp 1)/2} U_\pm(\tilde{\mathfrak{n}}_2, 2L + s - z)\, V_s(\tilde{\mathfrak{n}}_1, \tilde{\mathfrak{n}}_2, L) & \text{for} \quad z \in IV, \\ V_s(\tilde{\mathfrak{n}}_1, \tilde{\mathfrak{n}}_2, L)\, e^{ik_z[z-2L-s]} & \text{for} \quad z \in V, \end{cases} \tag{35}$$

where

$$V_\pm(\tilde{\mathfrak{n}}, z) := U_1(\tilde{\mathfrak{n}}, L) e^{ik_z z} \pm U_2(\tilde{\mathfrak{n}}, L) e^{-ik_z z}. \tag{36}$$

Note that Region *III* is absent for $s = 0$.

In order to acquire a better understanding of the behavior of singular waves, we examine the behavior of the corresponding time-averaged energy density and Poynting vector, $\langle u \rangle$ and $\langle \vec{S} \rangle$. Because the explicit expression for these quantities are rather complicated, in what follows we provide a graphical demonstration of their consequences and give their derivation in the appendix.

For convenience we respectively express the numerical values of $\langle u \rangle$ and $|\langle \vec{S} \rangle|$ in units of

$$\langle u_I \rangle := \frac{|b_1|^2}{2} \times \begin{cases} \epsilon_0 & \text{for TE waves,} \\ \mu_0 & \text{for TM waves,} \end{cases} \qquad |\langle \vec{S}_I \rangle| := \frac{|b_1|^2}{2} \times \begin{cases} Z_0^{-1} & \text{for TE waves,} \\ Z_0 & \text{for TM waves.} \end{cases} \tag{37}$$

These are the values of $\langle u \rangle$ and $|\langle \vec{S} \rangle|$ in Region I of Fig. 1, i.e., for $z < 0$.

It turns out that the presence of a gap between the gain and loss components of our system has drastic effects on the behavior of $\langle u \rangle$ and $\langle \vec{S} \rangle$. For this reason we examine the cases $s = 0$ and $s \neq 0$ separately.

Figures 8 and 9 show the plots of $\langle u \rangle$, $|\langle \vec{S} \rangle|$, and the angle between $\langle \vec{S} \rangle$ and the positive z-axis, i.e.,

$$\Theta := \arctan\left(\frac{\langle \vec{S} \rangle \cdot \hat{e}_x}{\langle \vec{S} \rangle \cdot \hat{e}_z} \right), \tag{38}$$

for singular TE and TM modes of a $\mathcal{PT}$-symmetric Nd:YAG bilayer slab ($s = 0$) obtained for the following values of the physical parameters.

$$L = 1 \text{ cm}, \qquad \eta = 1.8217, \qquad \theta = 30^\circ, \tag{39}$$

$$\lambda^{(E/M)} = 807.993 \text{ nm}, \qquad g^{(E)} = 10.851\,\text{cm}^{-1}, \qquad g^{(M)} = 11.244\,\text{cm}^{-1}. \tag{40}$$

As seen from these figures, $\langle u\rangle$ and $|\langle\vec{S}\rangle|$ oscillate throughout the gain and loss regions. As one increases z starting from zero, their envelope decreases slightly until they attain their minimum value at about $z = z_c := 0.9693$ mm for the TE mode and $z = z_c := 0.9354$ mm for the TM mode. For the values of z in the vicinity of z_c the direction of $\langle\vec{S}\rangle$ undergoes rapid changes, with Θ oscillating between 90° and 180° for $z < z_c$ and between 0° and 90° for $z > z_c$. This shows that $\langle\vec{S}\rangle$ always points away from the plane $z = z_c$, [41]. For $z \in (z_c, L)$ the envelops of $\langle u\rangle$ and $|\langle\vec{S}\rangle|$ increase steadily. In the lossy region, i.e., $z \in (L, 2L)$, they are monotonically decreasing functions of z. Furthermore, $\langle u\rangle$ and $|\langle\vec{S}\rangle|$ take much smaller values for $z > 2L$ compared with $z < 0$. Therefore, as expected, the emitted laser light from the outer boundary of the lossy layer has a smaller energy and power than the one emitted from that of the gain layer.

We have also examined the situation where θ exceeds the Brewster's angle θ_b. For a homogeneous gain slab, the condition $\theta > \theta_b$ implies that the time-averaged energy density $\langle u\rangle$ of the singular TM modes takes smaller values inside the slab than outside it [39]. This surprising effect is also present in the $\mathcal{PT}$-symmetric bilayer we are considering. For the singular TM modes with $\theta > \theta_b$, the value of $\langle u\rangle$ drops sharply as one enters either the gain or lossy layer from the outer boundary of the bilayer. But it then begins oscillating with a much larger amplitude than the magnitude of the difference of values of $\langle u\rangle$ inside and outside the bilayer. This is depicted in Fig. 10 where we offer a graphical comparison of $\langle u\rangle$ for the singular TE and TM modes obtained for the following values of the physical parameters.

$$\begin{aligned} &L = 1 \text{ cm}, \qquad \eta = 1.8217, \qquad \theta = 80^\circ, \\ &\lambda^{(E)} = 808.009 \text{ nm}, \qquad g^{(E)} = 9.025\,\text{cm}^{-1}, \\ &\lambda^{(M)} = 807.999 \text{ nm}, \qquad g^{(M)} = 9.903\,\text{cm}^{-1}. \end{aligned} \tag{41}$$

Next, we summarize the consequences of the presence of a gap between the gain and loss layers, i.e., $s > 0$:

1. Again there is a critical plane $z = z_c$ located inside the gain layer where $\langle u\rangle$ and $|\langle\vec{S}\rangle|$ attain their minimum value. Moreover, $\langle\vec{S}\rangle$ points away from this plane.

2. The behavior of the $\langle u\rangle$ and $|\langle\vec{S}\rangle|$ is highly sensitive to the ratio of s to

$$s_0 := \frac{\pi}{2k_z} = \frac{\lambda}{4\cos\theta}.$$

   If s/s_0 is an even integer, the presence of the gap does not lead to any significant changes in the behavior of $\langle u\rangle$ and $\langle\vec{S}\rangle$, and the situation resembles that of the case $s = 0$. In contrast, if s/s_0 is an odd integer, $\langle u\rangle$ and $|\langle\vec{S}\rangle|$ take much smaller values within the slabs and the gap in between, while they take larger values in the lossy layer and to its right. In other words, the emitted waves from the outer boundary of the lossy layer has larger energy density and power as compared to the case $s = 0$.

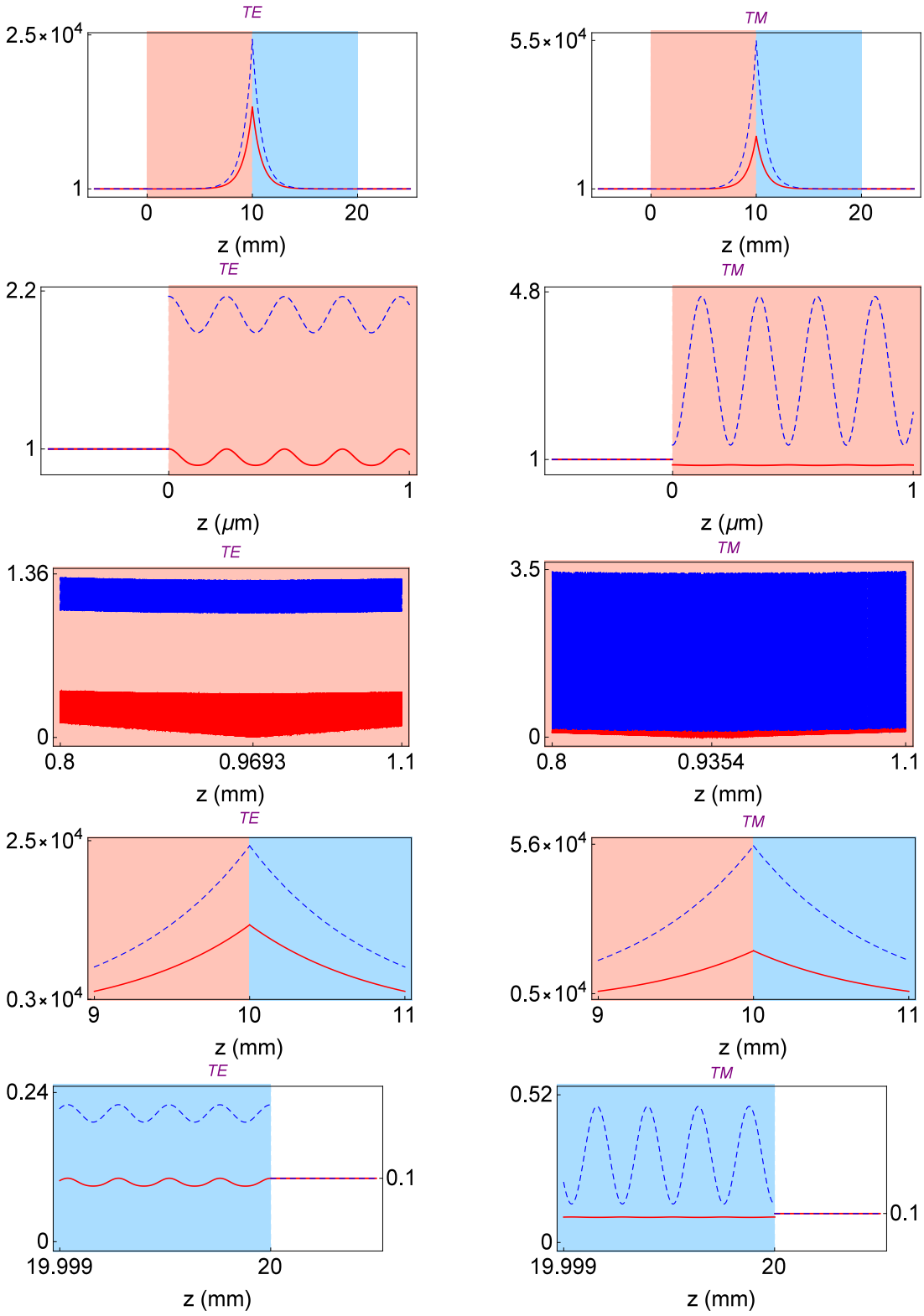

Figure 8: (Color online) Graphs of $\langle u\rangle$ in units of $\langle u_I\rangle$ (dashed navy curves) and $|\langle\vec{S}\rangle|$ in units of $|\langle\vec{S}_I\rangle|$ (solid red curves) for singular TE and TM modes of the $\mathcal{PT}$-symmetric Nd:YAG bilayer determined by (39) and (40). The pink and blue regions correspond to the layers with gain and loss, respectively.

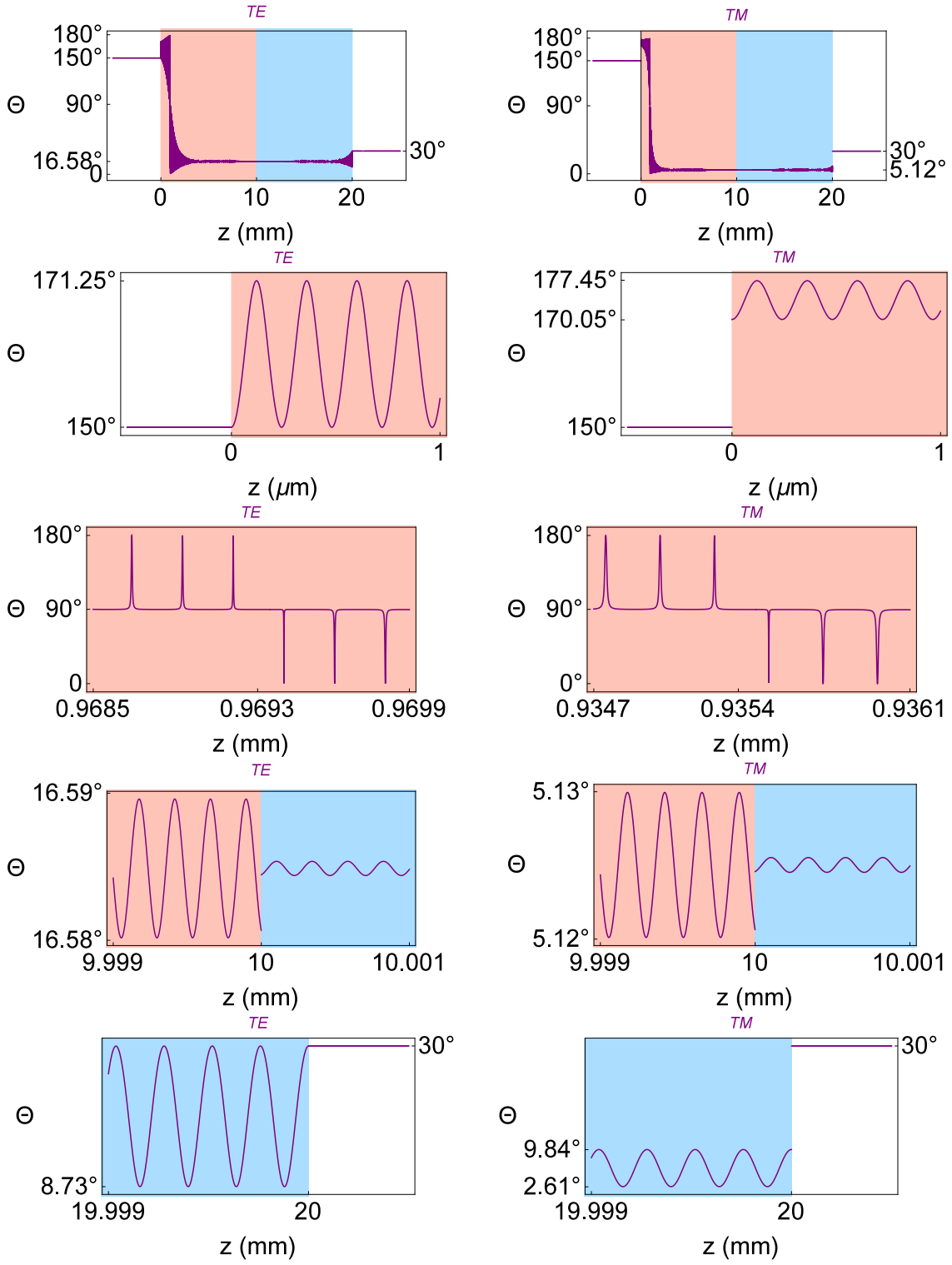

Figure 9: (Color online) Graphs of the angle Θ between the Poynting vector $\langle\vec{S}\rangle$ and positive z-axis for the same singular TE and TM modes as in Fig. 8. $\langle\vec{S}\rangle$ points away from the critical plane $z = 0.9693$ mm for the TE mode and $z = 0.9354$ mm for the TM mode.

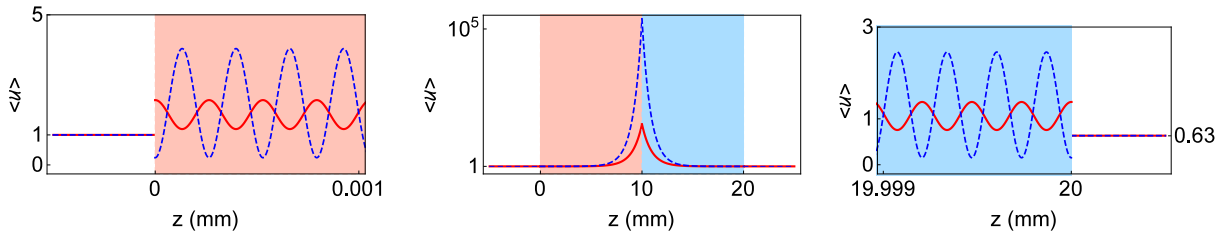

Figure 10: (Color online) Graphs of $\langle u\rangle$ (in units of $\langle u_I\rangle$) as a function of z for the singular TE (solid red curve) and TM (blue dashed curve) modes of a $\mathcal{PT}$-symmetric Nd:YAG bilayer slab with $\theta = 80^\circ > \theta_b$. The relevant physical parameters are given by (41). The pink and blue regions correspond to the layers with gain and loss, respectively.

The fact that for even values of s/s_0 the intensity of the waves inside the system can take extremely large values is due to the constructive interference of these waves. For this reason we use the terms 'constructive', 'destructive', and 'generic configurations' to refer to the cases with even, odd, and non-integer values of s/s_0, respectively.

The destructive configurations are more desirable, because for these configurations the waves interacting with the content of the slabs have much smaller intensities. Therefore the nonlinearities arising from this interaction are suppressed and the linear treatment of the problem that we offer is more reliable.

Figures 11-14 show the plots of $\langle u\rangle$, $|\langle\vec{S}\rangle|$, and the angle Θ of Eq. (38) for the singular TE and TM modes of a $\mathcal{PT}$-symmetric Nd:YAG two-slab system with the following specifications.

$$L = 25\ \text{mm}, \qquad \eta = 1.8217, \qquad \theta = 30^\circ, \tag{42}$$

$$\begin{cases} s^{(E/M)} = 20s_0 = 4.66\,\mu\text{m}, & \lambda^{(E/M)} = 807.996\ \text{nm}, \\ g^{(E)} = 3.8936\,\text{cm}^{-1}, & g^{(M)} = 4.1391\,\text{cm}^{-1}, \end{cases} \tag{43}$$

$$\begin{cases} s^{(E/M)} = 21s_0 = 4.90\,\mu\text{m}, & \lambda^{(E/M)} = 807.998\ \text{nm}, \\ g^{(E)} = 0.6366\,\text{cm}^{-1}, & g^{(M)} = 0.8626\,\text{cm}^{-1}, \end{cases} \tag{44}$$

$$\begin{cases} s^{(E/M)} = 21436.35s_0 = 5.00\,\text{mm}, & \lambda^{(E/M)} = 807.997\ \text{nm}, \\ g^{(E)} = 0.8291\,\text{cm}^{-1}, & g^{(M)} = 1.0756\,\text{cm}^{-1}. \end{cases} \tag{45}$$

Note that (43), (44), and (45) correspond to constructive, destructive, and generic configurations of the system, respectively.

We have also made a graphical analysis of the singular TE and TM modes of similar $\mathcal{PT}$-symmetric slab systems that are made of other material and for different values of θ. The results show no qualitative differences from those of the particular cases we have discussed above except that for sufficiently large values of θ the time-averaged energy density of the emitted waves from the lossy layer, $\langle u_V\rangle$, can take larger values than that for the emitted waves from the gain layer, $\langle u_I\rangle$. This surprising effect is present provided that the system is not in one of its constructive configurations, i.e., s is not an even multiple of s_0. It is most prevalent for the destructive configurations. Figure 15 provides a graphical demonstration of this behavior. It shows the plots of $\langle u\rangle$ for the TE and TM modes of a $\mathcal{PT}$-symmetric Nd:YAG two-slab system with the following

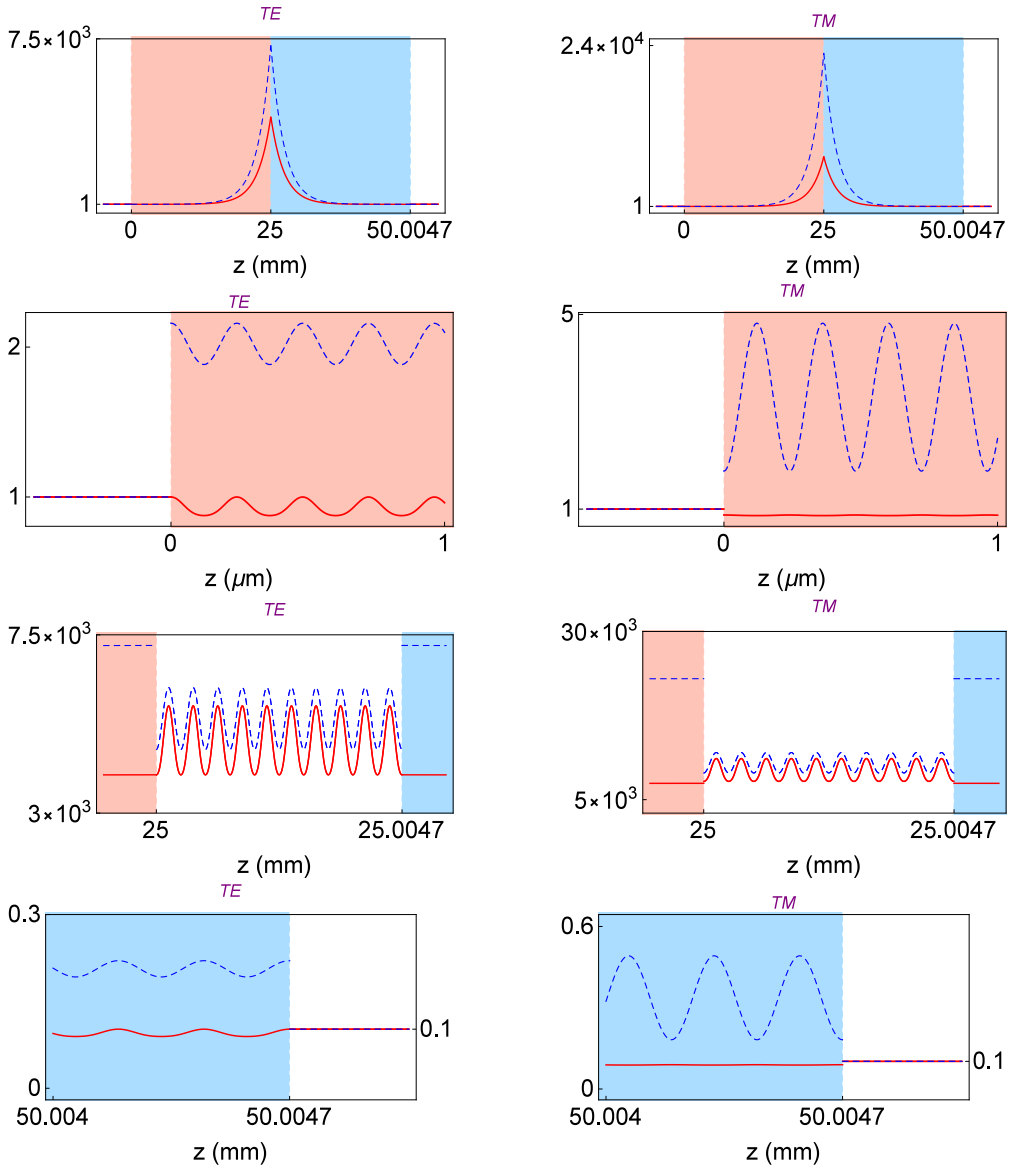

Figure 11: (Color online) Graphs of $\langle u \rangle$ in units of $\langle u_I \rangle$ (dashed navy curves) and $|\langle \vec{S} \rangle|$ in units of $|\langle \vec{S}_I \rangle|$ (solid red curves) for the singular TE and TM modes of the constructive configuration of a $\mathcal{PT}$-symmetric Nd:YAG two-slab system given by (42) and (43).

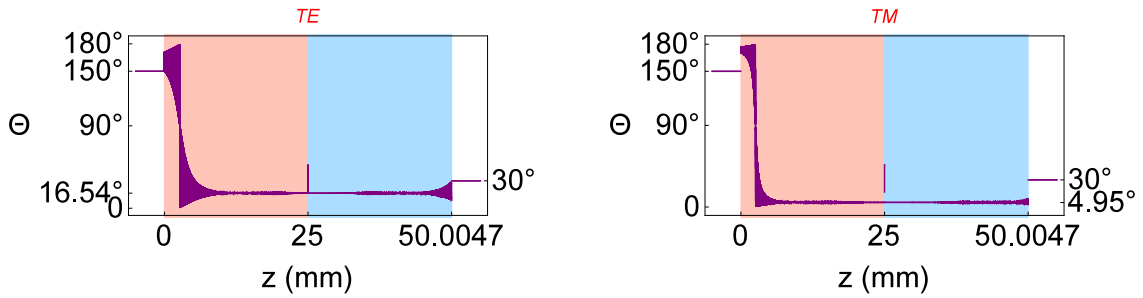

Figure 12: (Color online) Graphs of the angle Θ between the Poynting vector $\langle\vec{S}\rangle$ and positive z-axis for the TE and TM modes considered in Fig. 11. $\langle\vec{S}\rangle$ points away from the critical plane $z = 2.701$ mm for the TE mode and $z = 2.541$ mm for the TM.

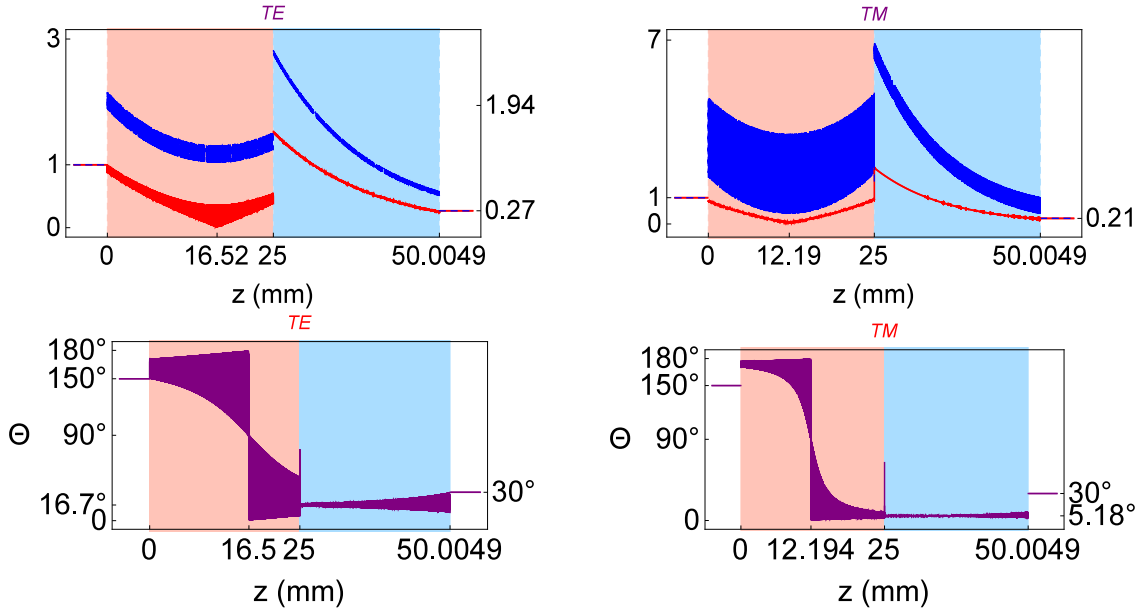

Figure 13: (Color online) Graphs of $\langle u\rangle$ in units of $\langle u_I\rangle$ (dashed navy curves) and $|\langle\vec{S}\rangle|$ in units of $|\langle\vec{S}_I\rangle|$ (solid red curves) on the top and the graphs of the angle Θ between $\langle\vec{S}\rangle$ and the positive z-axis in the bottom for the singular TE and TM modes of a destructive configuration of the $\mathcal{PT}$-symmetric Nd:YAG two-slab system with specifications (42) and (44). In contrast to the case $s = 0$, $\langle u\rangle$ and $|\langle\vec{S}\rangle|$ take much smaller values in the interior of the system.

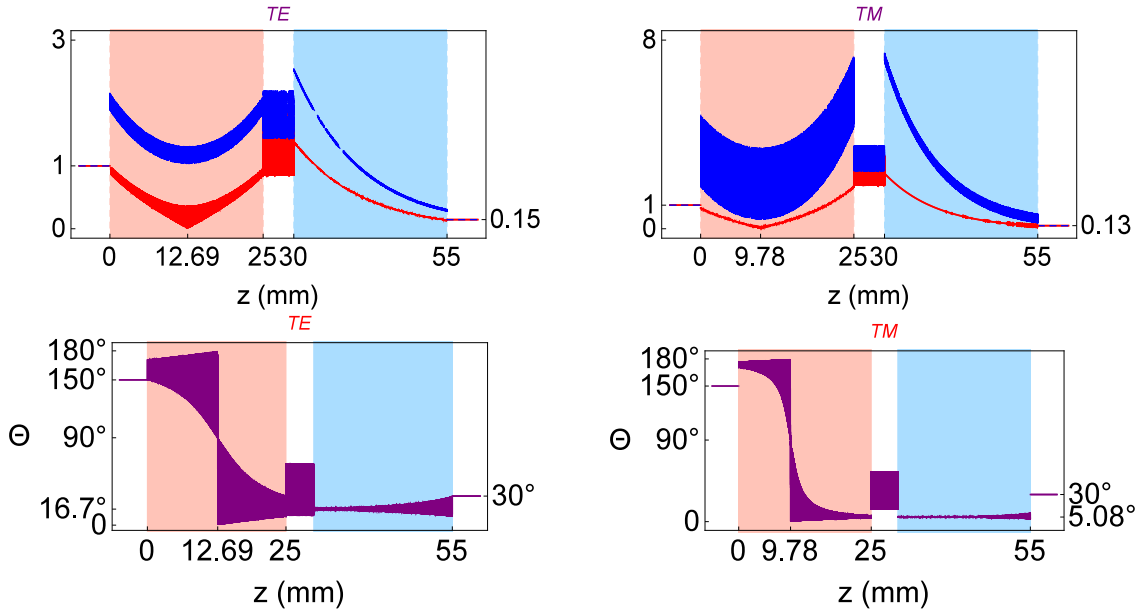

Figure 14: (Color online) Graphs of $\langle u\rangle$ in units of $\langle u_I\rangle$ (dashed navy curves) and $|\langle\vec{S}\rangle|$ in units of $|\langle\vec{S}_I\rangle|$ (solid red curves) on the top, and the graphs of the angle Θ between $\langle\vec{S}\rangle$ and the positive z-axis in the bottom for the singular TE and TM modes of a generic configuration of the $\mathcal{PT}$-symmetric Nd:YAG two-slab system with specifications (42) and (45).

values for the relevant physical parameters.

$$L = 25\ \text{mm}, \qquad \eta = 1.8217, \qquad \theta = 80^\circ, \tag{46}$$

$$\begin{cases} s^{(E/M)} = 20s_0 = 23.265\,\mu\text{m}, \\ \lambda^{(E)} = 807.996\ \text{nm}, & g^{(E)} = 2.656\,\text{cm}^{-1}, \\ \lambda^{(M)} = 808.000\ \text{nm}, & g^{(M)} = 5.140\,\text{cm}^{-1}, \end{cases} \tag{47}$$

$$\begin{cases} s^{(E/M)} = 21s_0 = 24.429\,\mu\text{m}, \\ \lambda^{(E)} = 808.032\ \text{nm}, & g^{(E)} = 0.109\,\text{cm}^{-1}, \\ \lambda^{(M)} = 807.998\ \text{nm}, & g^{(M)} = 0.394\,\text{cm}^{-1}, \end{cases} \tag{48}$$

$$\begin{cases} s^{(E/M)} = 4298.24s_0 = 5.000\,\text{mm}, \\ \lambda^{(E)} = 807.997\ \text{nm}, & g^{(E)} = 0.215\,\text{cm}^{-1}, \\ \lambda^{(M)} = 807.996\ \text{nm}, & g^{(M)} = 0.638\,\text{cm}^{-1}, \end{cases} \tag{49}$$

Clearly (47), (48), and (49) respectively correspond to the constructive, destructive, and generic configurations. Further examination shows that there is always a critical angle θ_c such that $\langle u_I\rangle \geq \langle u_V\rangle$ for $\theta \leq \theta_c$. For $\theta > \theta_c$, both $\langle u_I\rangle \geq \langle u_V\rangle$ and $\langle u_I\rangle < \langle u_V\rangle$ can occur. The latter case dominates for larger values of $\theta - \theta_c$.

Comparing the numerical values of the threshold gain coefficients listed in (43) – (45) and (47) – (49), we see that they are smaller for the destructive configurations than the generic and constructive ones. This reveals another advantage of destructive configurations for the purpose of using the system as a laser or a CPA. We have indeed checked that the peaks in the graphs of the

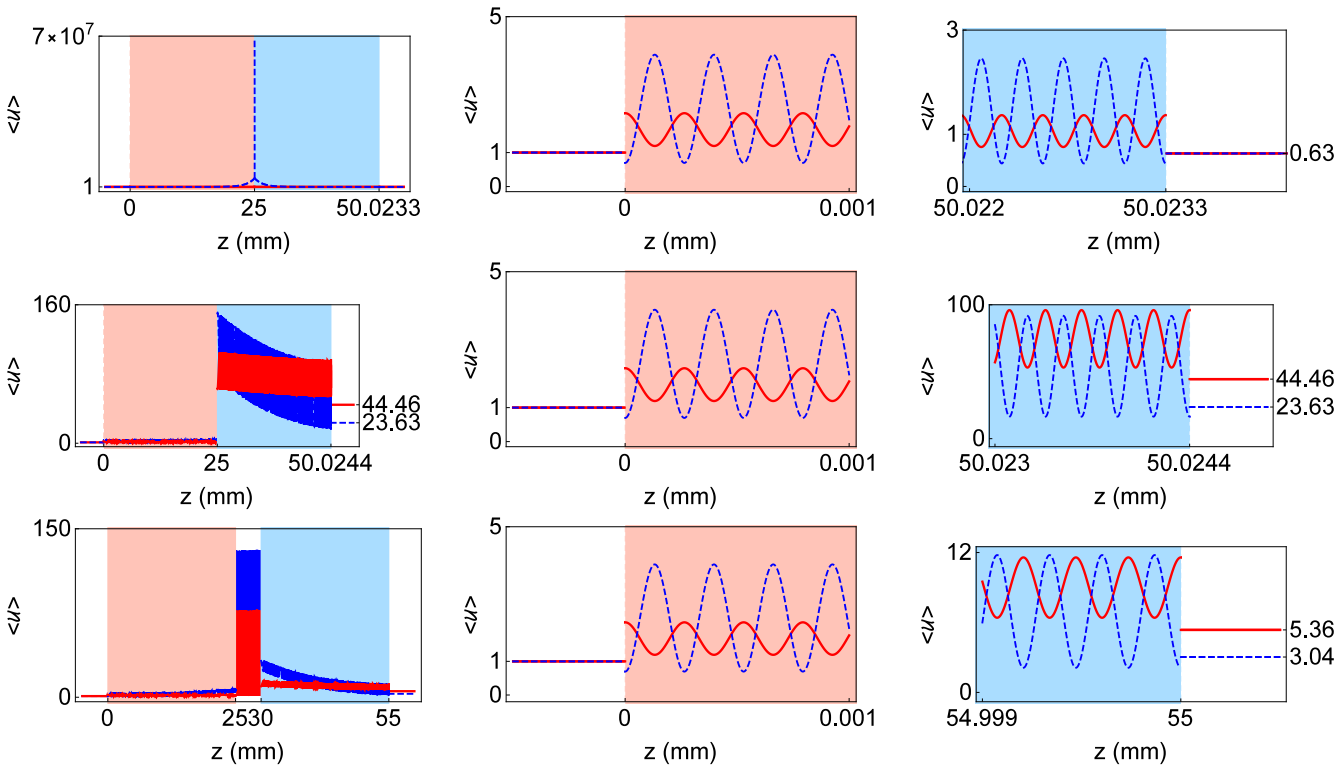

Figure 15: (Color online) Graphs of $\langle u \rangle$ (in units of $\langle u_I \rangle$) as a function of z for the singular TE (solid red curves) and TM (blue dashed curves) modes of a $\mathcal{PT}$-symmetric Nd:YAG two-slab system with specifications (46) – (49). Plots depicted in the top, middle, and bottom rows correspond to the constructive, destructive, and generic configurations given by (47), (48), and (49), respectively.

threshold gain coefficient that are given in Fig. 5 correspond to the constructive configurations of the system while their minima give the destructive configurations.

7 Amplitude and Phase Conditions for the CPA Action

An optical system functions as a CPA provided that the condition for the realization of a spectral singularity is realized for the time-reversed system. For a $\mathcal{PT}$-symmetric system this coincides with the condition for having a spectral singularity for the system itself. It is however important to notice that this is just a necessary condition. A system fulfilling this condition would absorb incoming waves only if they have appropriate amplitude and phase. For the $\mathcal{PT}$-symmetric slab systems we consider in this article, we have already derived the condition for the emergence of a spectral singularity. In what follows we determine the amplitude and phase conditions for the incoming waves that are absorbed by these systems.

Consider a $\mathcal{PT}$-symmetric slab system of the form depicted in Fig. 1 with $\mathfrak{n}_2 = \mathfrak{n}_1^* = \mathfrak{n}^*$. Suppose that the system supports a spectral singularity in a TE or TM mode with wavenumber k and angle θ. Then for $z \notin [0, 2L + z]$, i.e., outside the system, the electric field $\vec{E}(x, y, z)$ for the TE wave and the magnetic field $\vec{H}(x, y, z)$ for the TM wave have the form

$$\begin{cases} b_1 e^{i(k_x x - k_z z)} \hat{e}_y & \text{for } z \in I, \\ a_5 e^{i(k_x x + k_z z)} \hat{e}_y & \text{for } z \in V. \end{cases} \tag{50}$$

This in particular shows that, for $z \notin [0, 2L + z]$, the corresponding time-reversed waves that are absorbed by the time-reversed system are given by

$$\begin{cases} b_1^* e^{-i(k_x x - k_z z)} \hat{e}_y & \text{for } z \in I, \\ a_5^* e^{-i(k_x x + k_z z)} \hat{e}_y & \text{for } z \in V. \end{cases} \tag{51}$$

The time-reversed system is obtained by swapping the gain and loss layers, i.e., $\mathfrak{n} \to \mathfrak{n}^*$. In light of the equivalence between this operation and the reflection $z \to 2L + s - z$, we infer that the original system (where the gain component is to the left of the lossy one) would absorb waves of the form

$$\begin{cases} a_5^* e^{-ik_z(2L+s)} e^{-i(k_x x - k_z z)} \hat{e}_y & \text{for } z \in I, \\ b_1^* e^{ik_z(2L+s)} e^{-i(k_x x + k_z z)} \hat{e}_y & \text{for } z \in V. \end{cases} \tag{52}$$

In particular, the incidence angle at $z = 0$ is given by $-\theta$, where θ was the angle determining the singular TE and TM waves in the preceding sections. Figure 16 shows the emitted and absorbed waves given by (50) – (52).

Because b_1 is a free parameter, it is the ratio ρ of the complex amplitude of the incoming waves for $z \to 0$ and $z \to 2L + s$ that is crucial for their absorption by the system. In light of (30) and (52), this is given by

$$\rho = \frac{e^{-ik_z(2L+s)} a_5^*}{b_1^*} = V_s(\tilde{\mathfrak{n}}, \tilde{\mathfrak{n}}^*)^*, \tag{53}$$

where $V_s(\tilde{\mathfrak{n}}, \tilde{\mathfrak{n}}^*)$ is introduced in (31). In particular, the ratio of the amplitudes and phase factors for the incident waves from the left to that from the right are respectively given by

$$|\rho| = |V_s(\tilde{\mathfrak{n}}, \tilde{\mathfrak{n}}^*)|, \qquad e^{i\delta\phi} = \frac{V_s(\tilde{\mathfrak{n}}, \tilde{\mathfrak{n}}^*)^*}{|V_s(\tilde{\mathfrak{n}}, \tilde{\mathfrak{n}}^*)|}. \tag{54}$$

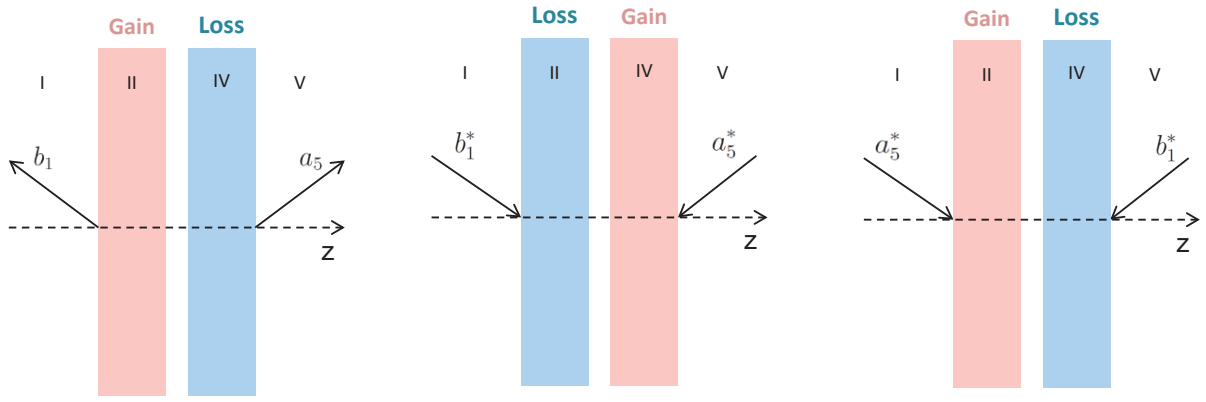

Figure 16: (Color online) The schematic description of the waves emitted by the CPA-laser as given by (50) on the left, the waves absorbed by the time-reversed system corresponding to (51) in the middle, and the waves absorbed by the original CPA-laser as quantified by (52) on the right.

Tables 4-6 give the numerical values of the physical parameters for which various configurations of our $\mathcal{PT}$-symmetric slab system perform as a CPA for different incident TE and TM waves.

	Bilayer	Construtive Conf.	Destructive Conf.	Generic Conf.
$s^{TE/TM}$	0	4.040 μm	4.242 μm	5.000 mm
κ^{TE}	-7.351×10^{-5}	-8.804×10^{-6}	-4.927×10^{-6}	-5.615×10^{-6}
κ^{TM}	-7.351×10^{-5}	-2.813×10^{-5}	-4.927×10^{-6}	-5.615×10^{-6}
g^{TE}	11.433 cm^{-1}	1.369 cm^{-1}	0.766 cm^{-1}	0.873 cm^{-1}
g^{TM}	11.433 cm^{-1}	4.375 cm^{-1}	0.766 cm^{-1}	0.873 cm^{-1}
λ^{TE}	808.006 nm	808.005 nm	807.100 nm	807.999 nm
λ^{TM}	808.006 nm	807.998 nm	807.998 nm	807.999 nm
$\lvert\rho^{TE}\rvert$	0.2912	0.2912	0.2515	0.2687
$\lvert\rho^{TM}\rvert$	0.2912	0.2912	0.2515	0.2687
$\delta\phi^{TE}$	93.058°	135.513°	90.022°	109.799°
$\delta\phi^{TM}$	93.058°	135.513°	90.022°	109.799°

Table 4: Physical parameters for the coherent perfect absorption of the TE and TM modes with incidence angle $\theta = 0°$. The constructive and destructive configurations correspond to the $s/s_0 = 10$ and $s/s_0 = 21$, respectively.

8 Concluding Remarks

The phenomenon of coherent perfect absorption of electromagnetic waves corresponds to the time-reversal of lasing at the threshold gain. The basic mathematical concept describing the latter is the spectral singularity of a complex scattering potential. Spectral singularities are given by the real zeros of the M_{22} entry of the transfer matrix of the potential, while their

	Bilayer	Construtive Conf.	Destructive Conf.	Generic Conf.
$s^{TE/TM}$	0	4.665 μm	4.898 μm	5.000 mm
κ^{TE}	-6.977×10^{-5}	-2.503×10^{-5}	-4.093×10^{-6}	-5.331×10^{-6}
κ^{TM}	-7.230×10^{-5}	-2.661×10^{-5}	-5.546×10^{-6}	-6.916×10^{-6}
g^{TE}	10.851 cm^{-1}	3.894 cm^{-1}	0.637 cm^{-1}	0.829 cm^{-1}
g^{TM}	11.244 cm^{-1}	4.139 cm^{-1}	0.863 cm^{-1}	1.076 cm^{-1}
$\lambda^{TE/TM}$	807.993 nm	807.996 nm	807.998 nm	807.997 nm
$\lvert\rho^{TE}\rvert$	0.3194	0.3194	0.5184	0.3812
$\lvert\rho^{TM}\rvert$	0.3194	0.3194	0.4604	0.3622
$\delta\phi^{TE}$	154.018°	131.050°	179.346°	151.612°
$\delta\phi^{TM}$	153.903°	130.996°	179.083°	152.690°

Table 5: Physical parameters for the coherent perfect absorption of the TE and TM modes with incidence angle $\theta = -30°$. The constructive and destructive configurations correspond to the $s/s_0 = 10$ and $s/s_0 = 21$, respectively.

	Bilayer	Construtive Conf.	Destructive Conf.	Generic Conf.
$s^{TE/TM}$	0	23.265 μm	24.429 μm	5.000 mm
κ^{TE}	-5.803×10^{-5}	-1.708×10^{-5}	-6.994×10^{-7}	-1.383×10^{-6}
κ^{TM}	-6.368×10^{-5}	-3.305×10^{-5}	-2.533×10^{-6}	-4.104×10^{-6}
g^{TE}	9.025 cm^{-1}	2.656 cm^{-1}	0.109 cm^{-1}	0.215 cm^{-1}
g^{TM}	9.903 cm^{-1}	5.140 cm^{-1}	0.394 cm^{-1}	0.638 cm^{-1}
λ^{TE}	808.009 nm	807.996 nm	808.032 nm	807.997 nm
λ^{TM}	807.999 nm	808.000 nm	807.998 nm	807.996 nm
$\lvert\rho^{TE}\rvert$	0.7959	0.7959	6.6679	2.3158
$\lvert\rho^{TM}\rvert$	0.7959	0.7959	4.8607	1.7425
$\delta\phi^{TE}$	89.733°	127.382°	179.738°	16.792°
$\delta\phi^{TM}$	95.976°	38.371°	176.942°	9.002°

Table 6: Physical parameters for the coherent perfect absorption of the TE and TM modes with incidence angle $\theta = -80°$. The constructive and destructive configurations correspond to the $s/s_0 = 10$ and $s/s_0 = 21$, respectively.

time-reversal correspond to the real zeros of M_{11}. Because for a $\mathcal{PT}$-symmetric potential these coincide, $\mathcal{PT}$-lasers act also as a coherent perfect absorber. Such a CPA-laser would absorb incident waves from the left and right directions only if they have correct amplitude and phase contrasts. In this article we have examined in great detail the conditions for achieving CPA-laser action in a $\mathcal{PT}$-symmetric slab system with adjacent or separated gain and loss layers. This is actually the simplest experimentally realizable model for a CPA-laser that allows for a completely analytic treatment.

Our results show that the presence of the separation between the gain and loss layers can have dramatic effects on the performance of this system as a CPA-laser. In particular if the separation distance s is an even integer multiple of a characteristic length scale, namely $s_0 := \pi/2\lambda\cos\theta$, the time-averaged energy density and the magnitude of the Poynting vector for the singular TE and TM waves take extremely large values inside the system. The opposite is the case when s is an odd integer multiple of s_0. These, so-called destructive configurations, provide the optimal situations where we can safely ignore the effects of nonlinearities and operate the system either as a laser or a coherent perfect absorber with smaller values of gain and loss.

Another outcome of our study is the counterintuitive observation that for nonconstructive configurations of the system the intensity of the emitted wave from the lossy layer can be larger than the one from its gain layer. This effect occurs for sufficiently large values of the incidence (emission) angle θ and is more prevalent for the destructive configurations.

We have also derived an explicit formula for the amplitude and phase contrast for the incoming waves that are absorbed by our CPA-laser, and given the numerical values of the physical quantities for which various configurations of the system function as a CPA. Again for nonconstructive configurations with large values of θ, we find that the intensity of the incoming wave that is absorbed by the gain layer can be larger than that of the wave absorbed by the lossy layer.

Note: After the completion of this project, we were made aware of Ref. [42] where the author explore prospects of an experimental realization of CPA-laser action in a similar non-$\mathcal{PT}$-symmetric system.

Acknowledgments: We are grateful to Ali Serpengüzel for fruitful discussions. This work has been supported by the Scientific and Technological Research Council of Turkey (TÜBİTAK) in the framework of the project no: 112T951, and by the Turkish Academy of Sciences (TÜBA).

Appendix: Poynting vector and energy density of the singular waves

By definition the time-averaged Poynting vector and energy density [43] are respectively given by

$$\langle\vec{S}\rangle = \frac{1}{2}\,\mathrm{Re}\left(\vec{E}\times\vec{H}^*\right), \tag{55}$$

$$\langle u\rangle := \frac{1}{4}\mathrm{Re}\left(\vec{E}\cdot\vec{D}^* + \vec{B}\cdot\vec{H}^*\right) = \frac{1}{4}\left(\epsilon_0\mathrm{Re}[\mathfrak{z}(z)]|\vec{E}|^2 + \mu_0|\vec{H}|^2\right), \tag{56}$$

where "Re" stands for the real part of its argument. In what follows we compute these quantities for the singular TE and TM modes of our slab system. This requires substituting the formulas given in Table 3 in Eqs. (55) and (56). The result is as follows. For $s = 0$,

$$\langle \vec{S}^{(E/M)} \rangle = |\langle \vec{S}_I^{(E/M)} \rangle| \times \begin{cases} \sin\theta\, \hat{e}_x - \cos\theta\, \hat{e}_z & \text{for} \quad z \in I, \\ \mathcal{Y}_0(\tilde{\mathfrak{n}}_1, z) \sin\theta\, \hat{e}_x + \mathcal{Z}_0^{(E/M)}(\tilde{\mathfrak{n}}_1, z) \cos\theta\, \hat{e}_z & \text{for} \quad z \in II, \\ \mathcal{X}_0(\tilde{\mathfrak{n}}_1, \tilde{\mathfrak{n}}_2, L) \big[\mathcal{Y}_0(\tilde{\mathfrak{n}}_2, 2L - z) \sin\theta\, \hat{e}_x & \\ \qquad - \mathcal{Z}_0^{(E/M)}(\tilde{\mathfrak{n}}_2, 2L - z) \cos\theta\, \hat{e}_z \big] & \text{for} \quad z \in IV, \\ \mathcal{X}_0(\tilde{\mathfrak{n}}_1, \tilde{\mathfrak{n}}_2, L) [\sin\theta\, \hat{e}_x + \cos\theta\, \hat{e}_z] & \text{for} \quad z \in V, \end{cases}$$

$$\langle u^{(E/M)} \rangle = \langle u_I^{(E/M)} \rangle \times \begin{cases} 1 & \text{for} \quad z \in I, \\ \mathcal{U}_0^{(E/M)}(\tilde{\mathfrak{n}}_1, z) & \text{for} \quad z \in II, \\ \mathcal{U}_0^{(E/M)}(\tilde{\mathfrak{n}}_2, 2L - z) \mathcal{X}_0(\tilde{\mathfrak{n}}_1, \tilde{\mathfrak{n}}_2, L) & \text{for} \quad z \in IV, \\ \mathcal{X}_0(\tilde{\mathfrak{n}}_1, \tilde{\mathfrak{n}}_2, L) & \text{for} \quad z \in V, \end{cases}$$

where the superscripts (E) and (M) refer to the TE and TM waves respectively, $|\langle \vec{S}_I^{(E)} \rangle| := |b_1|^2/2Z_0$, $|\langle \vec{S}_I^{(M)} \rangle| := Z_0|b_1|^2/2$, $\mathcal{X}_0(\tilde{\mathfrak{n}}_1, \tilde{\mathfrak{n}}_2, z) := |V_0(\tilde{\mathfrak{n}}_1, \tilde{\mathfrak{n}}_2, z)|^2$, $\mathcal{Y}_0(\tilde{\mathfrak{n}}, z) := \mathrm{Re}\left(\frac{\mathfrak{u}}{\tilde{\mathfrak{n}}}\right) |U_+(\tilde{\mathfrak{n}}, z)|^2$, $\mathcal{Z}_0^{(E)}(\tilde{\mathfrak{n}}, z) := \mathrm{Re}\left\{U_+(\tilde{\mathfrak{n}}, z) U_-^*(\tilde{\mathfrak{n}}, z)\, \mathfrak{u}^*\right\}$, $\mathcal{Z}_0^{(M)}(\tilde{\mathfrak{n}}, z) := \mathrm{Re}\left\{U_+^*(\tilde{\mathfrak{n}}, z)\, U_-(\tilde{\mathfrak{n}}, z)\, \mathfrak{u}\right\}$, $\langle u_I^{(E)} \rangle := \epsilon_0 |b_1|^2/2$, $\langle u_I^{(M)} \rangle := \mu_0 |b_1|^2/2$,

$$\begin{aligned} \mathcal{U}_0^{(E)}(\tilde{\mathfrak{n}}, z) &:= \frac{1}{2} \left\{ [\sin^2\theta\, + \mathrm{Re}(\mathfrak{n}^2)]\, \mathcal{Y}_0(\tilde{\mathfrak{n}}, z) + \cos^2\theta \mathcal{W}_0(\tilde{\mathfrak{n}}, z) \right\}, \\ \mathcal{U}_0^{(M)}(\tilde{\mathfrak{n}}, z) &:= \frac{1}{2} \left\{ \cos^2\theta\, \mathcal{W}_0(\tilde{\mathfrak{n}}, z) + \left[\left(\mathrm{Re}\left[\frac{\mathfrak{u}}{\tilde{\mathfrak{n}}} \right] \right)^{-1} + \sin^2\theta \right] \mathcal{Y}_0(\tilde{\mathfrak{n}}, z) \right\}, \\ \mathcal{W}_0(\tilde{\mathfrak{n}}, z) &:= \mathrm{Re}\left(\frac{\tilde{\mathfrak{n}}}{\mathfrak{u}} \right) |U_-(\tilde{\mathfrak{n}}, z)|^2\, |\mathfrak{u}|^2, \end{aligned}$$

and V_0 and $U_\pm$ are given by (31) and (34). For $s > 0$,

$$\langle \vec{S}^{(E/M)} \rangle \;=\; |\langle \vec{S}_I^{(E/M)} \rangle| \times \begin{cases} \sin\theta\, \hat{e}_x - \cos\theta\, \hat{e}_z & \text{for} \quad z \in I, \\ \mathcal{Y}_0(\tilde{\mathfrak{n}}_1, z) \sin\theta\, \hat{e}_x + \mathcal{Z}_0^{(E/M)}(\tilde{\mathfrak{n}}_1, z) \cos\theta\, \hat{e}_z & \text{for} \quad z \in II, \\ \mathcal{Y}_1(\tilde{\mathfrak{n}}_1, z - L) \sin\theta\, \hat{e}_x + \mathcal{Z}_1^{(E/M)}(\tilde{\mathfrak{n}}_1, z - L) \cos\theta\, \hat{e}_z & \text{for} \quad z \in III, \\ \mathcal{X}_s(\tilde{\mathfrak{n}}_1, \tilde{\mathfrak{n}}_2, L) \Big[\mathcal{Y}_0(\tilde{\mathfrak{n}}_2, 2L + s - z) \sin\theta\, \hat{e}_x & \\ \qquad - \mathcal{Z}_0^{(E/M)}(\tilde{\mathfrak{n}}_2, 2L + s - z) \cos\theta\, \hat{e}_z \Big] & \text{for} \quad z \in IV, \\ \mathcal{X}_s(\tilde{\mathfrak{n}}_1, \tilde{\mathfrak{n}}_2, L) [\sin\theta\, \hat{e}_x + \cos\theta\, \hat{e}_z] & \text{for} \quad z \in V, \end{cases}$$

$$\langle u^{(E/M)} \rangle \;=\; \langle u_I^{(E/M)} \rangle \times \begin{cases} 1 & \text{for} \quad z \in I, \\ \mathcal{U}_0^{(E/M)}(\tilde{\mathfrak{n}}_1, z) & \text{for} \quad z \in II, \\ \mathcal{U}_1(\tilde{\mathfrak{n}}_1, z - L) & \text{for} \quad z \in III, \\ \mathcal{X}_s(\tilde{\mathfrak{n}}_1, \tilde{\mathfrak{n}}_2, L)\, \mathcal{U}_0^{(E/M)}(\tilde{\mathfrak{n}}_2, 2L + s - z) & \text{for} \quad z \in IV, \\ \mathcal{X}_s(\tilde{\mathfrak{n}}_1, \tilde{\mathfrak{n}}_2, L) & \text{for} \quad z \in V, \end{cases}$$

where $\mathcal{X}_s(\tilde{\mathfrak{n}}_1,\tilde{\mathfrak{n}}_2,z):=|V_s(\tilde{\mathfrak{n}}_1,\tilde{\mathfrak{n}}_2,z)|^2$, $\mathcal{Y}_1(\tilde{\mathfrak{n}},z):=|V_+(\tilde{\mathfrak{n}},z)|^2$, $\mathcal{Z}_1^{(E)}(\tilde{\mathfrak{n}},z):=\mathrm{Re}\left\{V_+(\tilde{\mathfrak{n}},z)V_-^*(\tilde{\mathfrak{n}},z)\right\}$, $\mathcal{Z}_1^{(M)}(\tilde{\mathfrak{n}},z):=\mathrm{Re}\left\{V_-(\tilde{\mathfrak{n}},z)V_+^*(\tilde{\mathfrak{n}},z)\right\}$, and

$$\mathcal{U}_1(\tilde{\mathfrak{n}},z):=\frac{1}{2}\left[\cos^2\theta\,|V_-(\tilde{\mathfrak{n}},z)|^2+(1+\sin^2\theta)\,|V_+(\tilde{\mathfrak{n}},z)|^2\right].$$

References

[1] W. T. Silfvast, *Laser Fundamentals*, Cambridge University Press, Cambridge, 1996.

[2] A. Mostafazadeh, Phys. Rev. A **83**, 045801 (2011).

[3] M. A. Naimark, Trudy Moscov. Mat. Obsc. **3**, 181 (1954) in Russian, English translation: Amer. Math. Soc. Transl. (2), **16**, 103 (1960).

[4] For a list of mathematical literature on spectral singularities see the review articles G. Sh. Guseinov, Pramana J. Phys. **73**, 587 (2009) and [27].

[5] B. F. Samsonov, J. Phys. A **38**, L571 (2005).

[6] A. Mostafazadeh, J. Phys. A **39**, 13495 (2006).

[7] A. Mostafazadeh and H. Mehri-Dehnavi, J. Phys. A **42**, 125303 (2009)

[8] A. Mostafazadeh and A. Batal, J. Phys. A **37**, 11645 (2004).

[9] A. Mostafazadeh, Int. J. Geom. Meth. Mod. Phys. **7**, 1191 (2010); arXiv:0810.5643.

[10] A. Mostafazadeh, Phys. Rev. Lett. **102**, 220402 (2009).

[11] A. Mostafazadeh, Phys. Rev. A **80**, 032711 (2009).

[12] S. Longhi, Phys. Rev. B **80**, 165125 (2009) and Phys. Rev. A **81**, 022102 (2010).

[13] B. F. Samsonov, J. Phys. A **43**, 402006 (2010) and **44**, 392001 (2011).

[14] A. Mostafazadeh, Phys. Rev. A **83**, 045801 (2011); A. Mostafazadeh and S. Rostamzadeh, Phys. Rev. A **86**, 022103 (2012).

[15] A. Mostafazadeh and M. Sarisaman, Phys. Lett. A **375**, 3387 (2011).

[16] A. Mostafazadeh and M. Sarısaman, Proc. R. Soc. A **468**, 3224 (2012); Phys. Rev. A **87**, 063834 (2013); Phys. Rev. A **88**, 033810 (2013).

[17] A. Mostafazadeh, J. Phys. A **45**, 444024 (2012).

[18] F. Correa and M. S. Plyushchay, Phys. Rev. D **86**, 085028 (2012).

[19] L. Chaos-Cador and G. Garcia-Calderon, Phys. Rev. A **87**, 042114 (2013).

[20] G. R. Li, X. Z. Zhang, and Z. Song, Ann. Phys. (N.Y.) **349**, 288 (2014).

[21] R. Aalipour, Phys. Rev. A **90**, 013820 (2014).

[22] H. Ramezani, H.-K. Li, Y. Wang, and X. Zhang, Phys. Rev. Lett. **113**, 263905 (2014).

[23] A. Mostafazadeh, Phys. Rev. Lett. **110**, 260402 (2013) and Phys. Rev. A **87**, 063838 (2013).

[24] X. Liu, S. D. Gupta, and G. S. Agarwal1, Phys. Rev. A **89**, 013824 (2014).

[25] K. N. Reddy and S. Dutta Gupta, Optics Lett. **39**, 4595 (2014).

[26] A. Mostafazadeh, Stud. Appl. Math. **133**, 353 (2014).

[27] A. Mostafazadeh, Geometric Methods in Physics, Trends in Mathematics, edited by P. Kielanowski, P. Bieliavsky, A. Odzijewicz, M. Schlichenmaier, and T. Voronov (Springer, Cham, 2015) pp 145-165; arXiv: 1412.0454.

[28] Y. D. Chong, L. Ge, H. Cao, and A. D. Stone, Phys. Rev. Lett. **105**, 053901 (2010).

[29] S. Longhi, Phys. Rev. A **82**, 031801 (2010).

[30] S. Longhi, Physics **3**, 61 (2010); Phys. Rev. A **83**, 055804 (2011); and Phys. Rev. Lett. **107**, 033901 (2011).

[31] W. Wan, Y. Chong, L. Ge, H. Noh, A. D. Stone, and H. Cao, Science 331, 889 (2011).

[32] L. Ge, Y. D. Chong, S. Rotter, H. E. Türeci, and A. D. Stone, Phys. Rev. A **84**, 023820 (2011).

[33] A. Ruschhaupt, F. Delgado, and J. G. Muga, J. Phys. A **38**, L171 (2005).

[34] Z. H. Musslimani, K. G. Makris, R. El-Ganainy, and D. N. Christodoulides, Phys. Rev. Lett. **100**, 030402 (2008);

[35] K. G. Makris, R. El-Ganainy, D. N. Christodoulidesand and Z. H. Musslimani, Phys. Rev. Lett. **100**, 103904 (2008);

[36] C. E. Rüter, K. G. Makris, R. El-Ganainy, D. N. Christodoulides, M. Segev, and D. Kip, Nature Phys. **6**, 192 (2010).

[37] Z. Lin, H. Ramezani, T. Eichelkraut, T. Kottos, H. Cao, and D. N. Christodoulides, Phys. Rev. Lett. **106**, 213901 (2011).

[38] A. Mostafazadeh, Phys. Rev. A **87**, 012103 (2013).

[39] A. Mostafazadeh and M. Sarısaman, Phys. Rev. A **91**, 043804 (2015).

[40] A. Mostafazadeh, Phys. Rev. A **90**, 023833 (2014).

[41] For the homogeneous slab studied in Ref. [39] this was the case for the parallel bisecting plane.

[42] B. Baum, H. Alaeian, and J. Dionne, J. Appl. Phys. **117**, 063106 (2015).

[43] J. D. Jackson, *Classical Electrodynamics,* Wiley & Sons, New York, 1975.